Development of a Knudsen Cell Reactor for Measuring the Uptake of Atmospheric Gases on Particulate Matter

Thomas H. Rockhold, Jr.

Thesis submitted to the faculty of the Virginia Polytechnic Institute and State University in partial fulfillment of the requirements for the degree of

Master of Science
In
Chemistry

John R. Morris, Chair
Gary L. Long
James M. Tanko

April 20, 2011
Blacksburg, VA

Keywords: Volatile Organic Compounds, Uptake Coefficient, Ethanol, Knudsen Cell, Silicon Dioxide, Mineral Dust Aerosols

Development of a Knudsen Cell Reactor for Measuring the Uptake of Atmospheric Gases on Particulate Matter

Thomas H. Rockhold, Jr.

ABSTRACT

Heterogeneous reactions between mineral dust aerosols and gas phase volatile organic compounds have the potential to impact important atmospheric chemical processes. However, little is known about the uptake and reactivity of volatile organic compounds on particulates found in the environment. A Knudsen cell was designed and constructed for providing precise measurement of reaction probabilities within these systems. The instrument was validated through a series of experiments. After validating the Knudsen cell against several key benchmarks, the instrument was used to measure the uptake coefficient for ethanol on particulate silicon dioxide. The uptake coefficient of ethanol on silicon dioxide, a common compound in mineral dust aerosols, was determined to be 7×10^{-7}. Therefore, uptake of ethanol on silicon dioxide would be competitive with the loss of other volatile organic compounds on silicon dioxide, which show similar rates of uptake. The Knudsen cell was validated and measured the uptake of ethanol on silicon dioxide, and future work with the Knudsen cell will study the uptake of chemical warfare agent simulants on metal oxides.

Acknowledgements

I would like to thank Jesus Christ for the salvation and abundant life he has provided. Through my relationship with him, I am assured of my destiny. Second, I am extremely thankful to my parents, Tom and Pam Rockhold. Their encouragement and support have been essential for my success and perseverance during graduate school.

Next, I wish to thank my advisor, John Morris, for his guidance and support of my goals during my graduate career. He has taught me many essential skills that not only apply to research here in graduate school, but skills that will help me wherever I go after graduation.

My thanks go out to those who made the days of graduate school a little less stressful. Particularly let me thank the Morris group members, past and present: Will Alexander, Josh Uzarski, Wes Gordon, Jessica Lu, Erin Davis, Steve Burrows, Alec Wagner, Amanda Wilmsmeyer, Brandon Jeffrey, Yafen Zhang, Josh Abelard, and Dimitar Panayotov. I would like to also thank undergraduate researcher, Francesca Crivellari, for her work in the design of the Knudsen cell reactor.

Third, let me also thank the other members of my committee, Gary Long and James Tanko, for their guidance and helpful conversations on pertinent topics during my graduate career. I would also like to thank Tom Wertalik and Josh Layfield, whose expertise was greatly appreciated and aided my progress in this work immensely. My thanks are also extended to Jeff Castle who helped translate a crucial journal article from French to English.

Finally, to the many friends who were there for me during the hard times. There are too many to name, but you know who you are. Thank you again for your support.

Table of Contents

List of Figures

List of Tables

List of Acronyms

ConFlat™	CF
Cloud Condensation Nucleii	CCN
Dinitrogen Pentoxide	N_2O_5
Fourier Transform Infrared Spectroscopy	FTIR
Keyser-Moore-Leu Model	KML
Linear Mass Dependent Regime	LMD
Methacrolein	MAC
Methyl Vinyl Ketone	MVK
Mass Spectrometry	MS
Nitrate Radicals	NO_3
Nitric Acid	HNO_3
Nitrite	NO_2^-
Nitrogen Dioxide	NO_2
Nitrogen Monoxide	NO
Nitrous Acid	HONO
Outer Diameter	OD
Ozone	O_3
Relative Humidity	RH
Residual Gas Analyzer	RGA
Silicon Dioxide	SiO_2
Teragrams	Tg
Ultra High Vacuum	UHV
Ultra High Purity	UHP
Volatile Organic Compounds	VOC

Chapter 1

Introduction and Motivation

Thesis Statement

The goal of the research presented herein is to develop and perform benchmark tests on a Knudsen cell designed to measure the uptake probability of volatile organic compounds (VOCs) on atmospherically relevant particles.

1.1. Introduction

Interactions between atmospheric aerosols and chemical compounds, such as oxidants and VOCs, can impact crucial chemical processes that occur in the atmosphere. The chemistry that occurs in the atmosphere plays a major role in environmental processes that affect climate, precipitation patterns, and human health.[1,2] Interest is given to the chemical interactions involving mineral dust aerosols. The term mineral dust aerosols refer to particulate matter that originate from soil particles on the Earth's surface.[3] Wind and major soil disturbances such as deforestation are major pathways for the introduction of mineral dust aerosols into the atmosphere.[3] Mineral dust aerosols have the potential to act as reactive sinks of gas phase oxidants such as ozone (O_3) and nitrate radicals (NO_3). Long range transport of organic compounds is possible when the organics adsorb to the surface of mineral dust aerosols.[4-6] The impacts of the chemical reactions involving mineral dust aerosols are not fully understood and more information is needed to further understand these important reactions.

One way to study the reactions between mineral dust aerosols and gas phase species is through the use of a Knudsen cell. A Knudsen cell is an instrument that is designed to measure the uptake coefficients (γ) of gas phase species on different surfaces.[7-9] Uptake coefficients are

the probability of a reaction occurring when a gas molecule collides with a surface. (Equation 1.1)

$$\gamma = \frac{number\ of\ gas\ phase\ molecules\ that\ react\ with\ a\ surface}{number\ of\ gas\ phase\ molecules\ that\ hit\ the\ surface} \quad (1.1)$$

The larger the uptake coefficient, the higher the probability of the reaction occurring. A reaction with a higher likelihood of occurring can potentially have wide ranging effects on the chemical processes that occur in the atmosphere. A Knudsen cell has been constructed to study the uptake coefficients of heterogeneous reactions of atmospheric importance. One heterogeneous reaction pathway of significant importance to atmospheric chemistry involves the uptake of compounds on the surface of mineral dust aerosols.

1.2. Mineral Dust Aerosols

Over one third of the Earth's surface is covered in deserts and semi-arid regions, which serve as the main source of mineral dust aerosols.[10] The Earth's major deserts, including the Sahara and Gobi, are some of the largest contributors of mineral dust aerosols.[4,10] Strong winds blowing across these regions, excavations, and deforestation are some of the methods of introduction of mineral dust aerosols into the atmosphere.[3,4,11,12] On average, 800 – 2000 teragrams (Tg) of mineral aerosols are emitted each year, and twenty million metric tons of mineral dust aerosols are suspended in the atmosphere at any given time.[1,4,11] Mineral dust aerosols can stay suspended in the atmosphere for days or weeks at a time.[10,11] During their lifetimes, mineral dust aerosols move through the atmosphere on wind currents over large distances. There is evidence to show that mineral dust aerosols from the Sahara desert are carried across the Atlantic Ocean.[3,4,11] Mineral dust aerosols originate from the arid and semi-arid regions of the Earth, they can travel over long distances increasing the potential to impact multiple chemical processes.

Another factor that determines the effect of mineral dust aerosols on atmospheric chemistry is the chemical composition of the individual particles.[12] The most common elements in mineral dust aerosols are silicon, magnesium, sodium, calcium, aluminum, and iron.[13] At least one of the elements listed is present in a mineral dust aerosol particle, but ratios of element mixtures will vary depending on the source of the particle.[13] The origin source and size influence the composition of different particles.[10] There are two size categories of soil particles: silt and clay. Silt particles are typically 2-50 μm and include quartz (SiO_2) and calcite ($CaCO_3$) and several others. Clay particles, which are typically around 2 μm, include compounds such as kaolinite.[10] The compounds present in a mineral dust aerosols directly determine how it affects chemistry of the atmosphere.[12] Mineral dust aerosols have the potential to interact with solar radiation, moisture in the atmosphere, atmospheric oxidants, and organic compounds.[4]

1.2.1. Effects of Mineral Dust Aerosols

A natural balance is maintained between the amount of solar radiation the Earth reflects and absorbs. Any changes to this balance, negative or positive, are called radiative forcing and directly impact the temperature of the atmosphere.[1] Mineral dust aerosols affect the radiation balance differently than other types of aerosols. For example, black carbon and sulfate aerosols absorb and reflect solar radiation respectively.[1,14] Mineral dust aerosols do not absorb solar radiation very readily; however, mineral dust aerosols strongly absorb thermal radiation from the Earth's surface.[1,15,16] Sokolik et al.[15] estimated that mineral dust aerosols increase the amount of radiation absorbed over arid regions by around 20-40 W m^{-2}. Mineral dust aerosols increase the amount of thermal radiation from the Earth's surface that the atmosphere absorbs.

Mineral dust aerosols can serve as cloud condensation nuclei (CCN) through the adsorption of water on the surface of the particles.[14,17-20] Seisel et al.[21] studied the interaction of

water with mineral dust aerosols. Samples for this study were gathered at the Cape Verde Islands, and consisted of mineral dust from the Sahara desert. Characterization of the aerosol samples taken from this location revealed the samples contained quartz and potassic feldspars ($KAlSi_3O_8$).[10,22] The uptake coefficient of water on these dust samples was found to be $(4.2 \pm 0.7) \times 10^{-2}$, demonstrating that water readily absorbs to the surface of these dust aerosols. This study showed how mineral dust aerosols can act as CCN.[21] Modeling studies also suggest mineral dust aerosols have a role in the inhibition of cloud growth.[1,11,21,23] The absorption of thermal radiation by mineral dust aerosols is believed to reduce the occurrence of clouds where these aerosols are present. Absorption of thermal radiation results in an increase in temperature to a point where moisture can no longer efficiently condense to form clouds.[11] Atmospheric models proposed by Gasso et al.[11] showed a decreasing trend of hurricane formation in the Atlantic when mineral dust aerosols were more prevalent. Mineral dust aerosols can either inhibit or support the growth of clouds, but the process varies from region to region. Atmospheric oxidant species can also react with the surface of mineral dust aerosols.

1.2.2. Reactive Uptake of Oxidant Species on Mineral Dust Aerosols

1.2.2.1. Reactive Uptake of Ozone with Mineral Dust Aerosols

To determine the importance of a reaction between an atmospheric oxidant and mineral dust aerosols, the uptake coefficient of O_3 on mineral dust aerosols has been measured in previous research.[24-26] In the upper atmosphere, harmful solar radiation is scattered back into space by the ozone layer. Loss of ozone to mineral dust aerosols can lead to detrimental effects on climate.[25] Michel et al.[25] studied the reactions of ozone on various mineral dust aerosols with a Knudsen cell reactor coupled to a mass spectrometer. Samples included in the study were SiO_2, α-Fe_2O_3, α-Al_2O_3, and dust samples from the Saharan desert and China loess. O_3 was

irreversibly lost to the surface of each sample studied except for the dust samples from China and the Sahara desert. During the studies of the dust samples containing China loess and Sahara dust, a slight recovery of O_3 signal in the mass spectrometer was observed. The signal recovery indicated the surface of the samples may have been contaminated. The observed uptake coefficients of O_3 determined in this research are summarized in Table 1.1.[25]

Table 1.1 – Observed uptake data from Michel et al.[25] The Saharan dust was ground up during the sample preparation phase. α-Al_2O_3 was the most reactive sample tested in this study

Sample	$\gamma_{o,BET}$
α-Al_2O_3 (25 μm particle size)	$(1.4 \pm 0.3) \times 10^{-4}$
α-Fe_2O_3	$(2.0 \pm 0.3) \times 10^{-4}$
SiO_2	$(6.3 \pm 0.9) \times 10^{-5}$
Saharan Dust (ground)	$(6 \pm 2) \times 10^{-5}$
China loess	$(2.7 \pm 0.8) \times 10^{-5}$

The uptake coefficients measured for O_3 on mineral dust aerosols are smaller than those determined for O_3 uptake on other surfaces found in the atmosphere.[25,27] O_3 is catalytically decomposed on the mineral dust aerosols studied here. The catalytic mechanism driving the loss of O_3 on the surface of the mineral dust aerosols could make these reactions more important than they seem.

O_3 molecules are more likely to encounter a weathered mineral dust aerosol particle that has interacted with inorganic and organic compounds than a clean particle in the atmosphere.[26] Weathered mineral dust aerosol particles can react differently with O_3.[25] Usher et al.[26] demonstrated how processed i.e. weathered mineral dust aerosols react differently from non-processed aerosols. α-Al_2O_3 powder was processed with nitric acid and sulfur dioxide to produce surface adsorbed nitrate and sulfite/bisulfate species respectively. SiO_2 powder was placed in either a solution of toluene with 7-oct-1-enyltrichlorosilane or n-octyltrichlorosilane and pyridine. The solutions used in the functionalization of SiO_2 resulted in powders with eight

carbon chain alkanes or alkenes adsorbed on the surface. The uptake coefficients of ozone (Table 1.2) on the alkene functionalized SiO_2 particles and sulfite/bisulfite covered α-Al_2O_3 increased. Increased uptake coefficients were a result of ozone reacting with the surface adsorbed species on these particles.

Table 1.2 – Summary of uptake coefficients for various samples from Usher et al.[26] O_3 uptake increased for samples with sulfite and alkene species.

Sample	$\gamma_{o,BET}$
α-Al_2O_3	$(1.2 \pm 0.4) \times 10^{-4}$
α-Al_2O_3 (Treated with HNO_3)	$(3.4 \pm 0.6) \times 10^{-5}$
α-Al_2O_3 (Treated with SO_2)	$(1.6 \pm 0.2) \times 10^{-4}$
SiO_2	$(5 \pm 1) \times 10^{-5}$
SiO_2 (C_8-alkane)	$(3 \pm 1) \times 10^{-5}$
SiO_2 (C_8-alkene)	$(7 \pm 2) \times 10^{-5}$

The uptake coefficients measured in this study showed the effect atmospheric processing has on the reactivity of mineral dust aerosols. Mineral dust aerosols processed by organic and inorganic compounds in the atmosphere have been shown to have very different chemistry than their unprocessed counterparts.[26] Other atmospheric oxidants, such as nitrogen dioxide (NO_2), nitric acid (HNO_3), and nitrate radicals (NO_3), can react with mineral dust aerosols.

1.2.2.2. Reactive Uptake of NO_2, HNO_3, and NO_3 on Mineral Dust Aerosols

Mineral dust aerosols can act as reactive sinks for atmospheric species such as NO_2, HNO_3, and NO_3. These reactions have been studied previously.[28-35] Underwood et al.[29] investigated how mineral dust aerosols react with nitrogen dioxide (NO_2). Using a Knudsen cell, several different mineral dust aerosols, including SiO_2, α-Al_2O_3, α-Fe_2O_3, and CaO, were exposed to NO_2. For all samples, except SiO_2, the reaction between NO_2 and the oxide surface resulted in surface adsorbed nitrite (NO_2^-). The adsorbed NO_2^- reacted with another surface bound NO_2^- to form nitrate (NO_3^-).[29,36] The uptake of NO_2 on the mineral dust aerosols studied here was determined to be 9.1×10^{-6}, 7.7×10^{-6}, and 2.2×10^{-5} for α-Al_2O_3, α-Fe_2O_3, and CaO

respectively.[29] Mineral dust aerosols were shown based on the calculated uptake coefficients, to not be competitive sinks for NO_2.

SiO_2 showed no measurable uptake for NO_2 under the conditions in the study presented above, but if the SiO_2 surface is hydrated, the interaction between SiO_2 and NO_2 changes.[30,31] Fourier transform infrared spectroscopy (FTIR) studies performed on a hydrated SiO_2 surface showed NO_2 reacts with adsorbed water to form surface adsorbed HNO_3.[30,31] HNO_3 was confirmed by the presence of absorption bands at 1677, 1399, 1315 cm^{-1}. Knudsen cell studies revealed that gas phase nitrous acid (HONO) was a product of the reaction of NO_2 with adsorbed water on the SiO_2 surface. This reaction is defined below. (Reaction 1.A)[30,31]

$$2NO_2\ (g) + H_2O\ (ads.) \rightarrow HNO_3\ (ads.) + HONO\ (g) \qquad (1.A)$$

Reaction 1.A is too slow in the gas or aqueous phases to be an important production source of HONO, and the heterogeneous reaction rate is expected to be faster and a more important contributor to gas phase HONO. Dry SiO_2 showed no reactive uptake of NO_2, but adsorbed water on the SiO_2 surface increased the reactivity of the surface.[30,31] The reaction between NO_2 and hydrated SiO_2 was shown to be a major contributor of gas phase HONO to the atmosphere.

The loss of HNO_3 on the surface of mineral dust aerosols was studied to determine the significance of such an interaction would have on atmospheric chemistry.[28,29,32,33] The results of these studies showed the reaction of HNO_3 and mineral dust aerosols was reversible on SiO_2. HNO_3 hydrogen bonded to the terminal hydroxyl groups on the SiO_2 surface, but the hydrogen bonds were not strong enough to effectively trap the HNO_3.[32] On the other mineral dust aerosols, α-Al_2O_3, MgO, CaO, Fe_2O_3, tested in these studies, the uptake of HNO_3 was irreversible and resulted in a surface coated with NO_3^-. (Reaction 1.B)[32]

$$HNO_3\ (g) \rightarrow [HNO_3\ (ads.)] \rightarrow H^+\ (ads) + NO_3^-\ (ads) \qquad (1.B)$$

Dissociation of the adsorbed HNO_3 on these surfaces resulted in the formation of surface adsorbed water.[32] The true uptake coefficients of HNO_3 on mineral dust aerosols are shown in Table 1.3.

Table 1.3 – True uptake of HNO_3 on various mineral dust aerosols determined by Underwood et al.[28,29]

Sample	γ_t
α-Al_2O_3	$(9.7 \pm 0.5) \times 10^{-5}$
SiO_2	$(2.9 \pm 0.2) \times 10^{-5}$
MgO	$(3.7 \pm 0.2) \times 10^{-4}$
Fe_2O_3	$(5.3 \pm 0.3) \times 10^{-5}$
CaO	$(6.1 \pm 0.3) \times 10^{-3}$

The uptake coefficients measured in Table 1.3 show that HNO_3 is lost to the surface of the mineral dust aerosols studied here, and in the presence of water the uptake of HNO_3 increased up to 50 times more than the uptake on dry surfaces.[28] The loss of HNO_3 through mineral dust aerosols was observed to be significant enough to have broader impacts on atmospheric chemistry.[32]

NO_3 is one of the most potent atmospheric oxidants.[1] Dentener et al.[34,35] have modeled the impact mineral dust aerosols have on the loss of NO_3 and dinitrogen pentoxide (N_2O_5). Models proposed by Dentener[34] suggested that under dry conditions the uptake of NO_3 and N_2O_5 on mineral dust aerosols is negligible, but the researchers stated the mechanism for NO_3 uptake on mineral dust aerosols is not well understood.[34] The goal of our future work in the Knudsen cell is to study the uptake of NO_3 and N_2O_5 on mineral dust aerosols. The NO_3/N_2O_5 source developed in Chapter 4 will be used in our future Knudsen cell studies.

1.2.2.3. Reactive Uptake of OH Radicals and Other Gas Species on Mineral Dust Aerosols

Modeling and experimental studies have looked at the uptake of OH_x species and SO_2 on mineral dust aerosols.[34,37,38] Dentener et al.[34] modeled the reactions of OH_x species on mineral dust aerosols. The results suggested that HO_x species with an odd number of hydrogen atoms,

OH and HO_2 radicals, would be lost on the surface of mineral dust particles. Reaction pathways involved in the reactive uptake of the HO_x are redox reactions of metals present in the particle such as iron. The influence of these interactions on the overall atmospheric budget of OH_x species was shown to be insignificant.[34] Usher et al.[37] studied the reactive uptake of SO_2 on various mineral dust aerosols including: TiO_2, $CaCO_3$, α-Fe_2O_3, MgO, α-Al_2O_3, and SiO_2. The true uptake coefficients calculated in this study for each sample is shown in Table 1.4. All of the samples tested in this study showed appreciable uptake of SO_2 except for SiO_2.

Table 1.4 – True uptake averages for the mineral dust aerosols studied in Usher et al.[37] All but SiO_2 showed appreciable uptake of SO_2

Sample	$\gamma_{o,BET}$
TiO_2	$(1.0 \pm 0.2) \times 10^{-4}$
$CaCO_3$	$(1.4 \pm 0.7) \times 10^{-4}$
α-Fe_2O_3	$(7.0 \pm 2) \times 10^{-5}$
MgO	$(5.1 \pm 0.5) \times 10^{-4}$
α-Al_2O_3	$(1.6 \pm 0.5) \times 10^{-4}$
SiO_2	$< 1 \times 10^{-7}$

FTIR analysis of the samples showed adsorbed sulfite (SO_3^{-2}) and bisulfite (HSO_3^-) on the surface of the samples after exposure to SO_2. The sulfite and bisulfite resulted from the oxidation of the SO_2 gas by the surface oxygen or hydroxyl groups on these mineral dust surfaces. In the case of $CaCO_3$, calcium sulfite was the product of surface oxidation of SO_2. The loss of SO_2 on mineral dust aerosols was found to be comparable to the gas phase loss of SO_2 in the atmosphere.[37] The research presented in Chapter 3 focuses on the uptake of VOCs on SiO_2, a common mineral dust aerosol.

1.3. Volatile Organic Compounds

All vapor phase organic compounds, except CO and CO_2, are classified as VOCs.[3] A wide variety of organic compounds have been identified in the atmosphere (Table 1.5) including normal alkanes, alcohols, and organic acids.[3,39] Humans contribute roughly 478 teragrams of

carbon per year (TgC yr^{-1}) through fuel combustion, biomass burning, and dumping of organic solvents. Churning of the oceans and emissions from vegetation introduce nearly 1,330 TgC yr^{-1}. The combined emission pathways result in nearly 1,808 TgC yr^{-1} of organic compounds released into the atmosphere.[39]

Table 1.5 – List of some of the VOCs present in the atmosphere.[3,39]

Volatile Organic Compound	Example(s)
Alkanes	methane, ethane
Alkenes	ethene, propene
Aromatics	benzene
Alcohols	methanol, ethanol
Ketones	acetone
Organic Acids	formic acid, acetic acid

The three most important oxidants in the atmosphere, OH radicals, O_3, and NO_3, have the strongest interactions with VOCs.[39] Reactions between VOCs and these oxidants can produce equally or more reactive species to further change the chemistry in the atmosphere.[39] Alkanes for instance produce water and nitric acid as a result of reactions with OH radicals and NO_3 respectively. Alkyl radicals are also a product of reactions with alkanes and OH and NO_3 radicals, and these alkyl radicals react further with O_2 and NO_x species to produce peroxynitrates.[39] Radical production is a common outcome for reactions between other VOCs and atmospheric oxidants.

Reactions between alcohols and atmospheric oxidants are of interest to this work because the research presented in Chapter 3 focuses on the reactive uptake of ethanol on mineral dust aerosols. Ethanol is present in the troposphere at a concentration of 40-70 ppt and has an atmospheric lifetime of 4 days.[3] Ethanol is known to react with gas phase OH radicals. The mechanism that drives reactions involving ethanol and OH radicals in the atmosphere involves hydrogen abstraction, and ethanol has three potential sites for the loss of a hydrogen atom.(Reactions 1.C – 1.E)[3]

$$OH\bullet + CH_3CH_2OH \rightarrow H_2O + \bullet CH_2CH_3OH \quad (5\%) \quad (1.C)$$
$$OH\bullet + CH_3CH_2OH \rightarrow H_2O + CH_3\dot{C}HOH \quad (90\%) \quad (1.D)$$
$$OH\bullet + CH_3CH_2OH \rightarrow H_2O + CH_3CH_2O\bullet \quad (5\%) \quad (1.E)$$

In the presence of NO, the overall reaction of ethanol with OH radicals results in the production of NO_2, hydroxy-acetaldehyde, formaldehyde, acetaldehyde, HO_2 and water.[3] To our knowledge, the loss of ethanol on mineral dust aerosols has not been studied. We present one of the first studies in Chapter 3 of the reaction of ethanol with SiO_2. The goal of this study is to not only test the Knudsen cell but also determine how important the reaction between ethanol and SiO_2 is to the overall chemistry of the atmosphere.

1.3.1. Interactions between Volatile Organic Compounds and Mineral Dust Aerosols

Through the determination of uptake coefficients of VOCs on mineral dust aerosols, the influence these reactions have on the atmosphere is determined.[5,6,40-49] Adsorption of VOCs on mineral dust aerosols not only remove the VOC from the atmosphere but create the possibility for long range transport of these organic compounds to areas where they are not found.[5,6] VOCs adsorbed on the surface of mineral dust aerosols can react with gas phase oxidants, thereby changing the concentrations of these oxidants. Changes in the concentrations of atmospheric oxidants could have a dramatic impact on atmospheric chemistry.[5,41] For these reasons, scientific studies seek to understand the role mineral dust aerosols have on atmospheric chemistry.

Kai-Uwe Goss comprehensively studied the interaction of VOCs with mineral dust aerosols.[6,42-45] Goss focused on the adsorption constants of these gases on various mineral dust aerosols present in the atmosphere. Adsorption constant (K) is defined in Equation 1.2 and is measured based on the retention time of the organic vapor through the column.[45]

$$K = \frac{volume\ of\ organic\ vapor\ per\ surface\ area}{volume\ organic\ vapor\ per\ volume\ of\ air} = \frac{(\frac{m^3}{m^2})}{(\frac{m^3}{m^3})} = \frac{m^3}{m^2} \quad (1.2)$$

The chromatography columns Goss used were packed with mineral dust aerosols including quartz (SiO_2), α-Al_2O_3, and $CaCO_3$. The adsorption constants of 50 different organic vapors were determined at different relative humidites (RH) in this study, and a small sample of the data is shown in Table 1.6.[45]

Table 1.6 – Adsorption constants of non polar and polar organic vapors for the three solid phases studied by Goss et al.[45] The adsorption constant of ethanol increases at 97% humidity for each surface tested.

	K (RH 45%)	K (RH 70%)	K (RH 90 %)	K (RH 97%)
SiO_2 (Quartz)				
n-Octane	1.35×10^{-5}	4.02×10^{-6}	1.52×10^{-6}	1.05×10^{-6}
Ethanol	2.86×10^{-4}	1.26×10^{-4}	6.82×10^{-5}	1.67×10^{-4}
α-Al_2O_3				
n-Octane	1.60×10^{-6}	1.01×10^{-6}	7.03×10^{-7}	5.74×10^{-7}
Ethanol	2.33×10^{-4}	1.23×10^{-4}	8.87×10^{-5}	9.22×10^{-5}
$CaCO_3$				
n-Octane	2.0×10^{-6}	1.41×10^{-6}	9.06×10^{-7}	7.57×10^{-7}
Ethanol	2.45×10^{-4}	1.39×10^{-4}	9.59×10^{-5}	1.06×10^{-4}

The adsorption constants depended on the humidity and the polarity of the organic vapor of a certain experiment. For non polar compounds, the adsorption constant continually decreased with increasing humidity; however, for polar compounds the adsorption constant decreased initially but above 97% RH the adsorption constant increased. The increase in the adsorption constant was theorized to be a result of the accumulation of water monolayers on the mineral dust aerosols. At 97% humidity, the van der Waals interactions between the water monolayers and the mobile phase are equivalent to a bulk water surface.[45] The adsorption constants measured in this study showed the strong adsorption of VOCs to mineral dust aerosols, but also the effect, both negative and positive, water has on the adsorption of VOCs on mineral dust aerosols.[6]

Grassian et al.[5,40,46,48-50] has studied the interactions between VOCs and mineral dust aerosols with a Knudsen cell reactor. The goal of these studies was to determine the uptake

coefficient (γ) of VOCs on various mineral dust aerosols. Uptake coefficient is defined as the loss of gas phase molecules per second divided by the number of gas-surface collisions per second.[5,24,26,28-30,37,40,46,50] The equation for uptake coefficient is explained in greater detail in Chapter 3. Samples of various masses were prepared and loaded into the Knudsen cell to be pumped down overnight. The overnight pump down was done in order to remove water on the surface of the samples, which Goss showed plays a role in the interaction of VOCs and mineral dust aerosols.[45] The change in mass spectrometer signal intensity for each VOC studied was used to determine the uptake coefficient for that particular system. Observed uptake coefficient (γ_{obs}) was plotted against the different masses of each sample as shown in Figure 1.1.

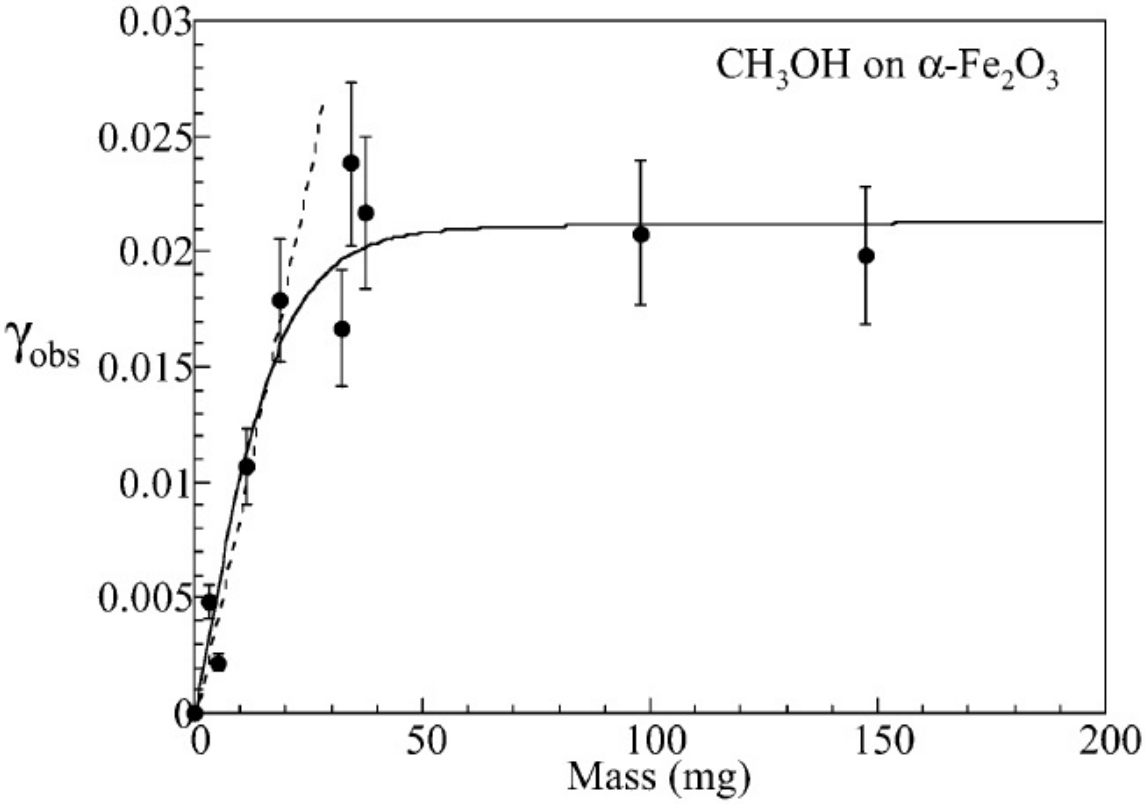

Figure 1.1 – Observed uptake of methanol plotted against different sample masses of α-Fe_2O_3. A linear increase in uptake is observed for small masses (Linear Mass Dependent regime) until the observed uptake levels out. The slope of the dotted line is used to determine the true uptake of the VOC on the surfaces.[5] Reprinted with permission from Carlos-Cuellar et al.[5] Copyright 2003 American Chemical Society

Initially, the observed uptake increases linearly with sample mass, but as sample mass increases the surface area increases and the layer height of the particles increases as well. At a certain point the VOC can only diffuse into the surface so far thereby accounting for the plateau effect observed in this study and other studies done by Grassian.[5,24,25,28,30,33,40,50] The mass dependent trend of observed uptake was observed for each sample/VOC combination studied here.

The observed uptake coefficient does not take into effect diffusion of the reactive gas into the powder samples studied by Grassian et al. When the gas diffuses into the powder the surface area for which the gas has access to on the sample increases.[5] The true uptake coefficient (γ_t) factors in the diffusion of the gas into a porous surface. The true uptake coefficient of VOCs on mineral oxides can be calculated one of two ways. The first method to calculate true uptake is with the Keyser-Moore-Leu (KML) model.[51,52] The model is based on the diffusion of gas molecules into porous solids during heterogeneous reactions.[51,52] Diffusion of gas molecules into a porous surface results in the surface area of the particles on the upper and lower layers having a role in the true uptake of the gas on the surface.[5] Carlos-Cuellar et al. fitted their data to Equation 1.3.[5] The solid line in Figure 1.1 was the result of the data fitting.

$$\gamma_{obs} = \gamma_t \rho_b S_{BET}(h_e + \eta h_i) \quad (1.3)$$

The terms in the above equation were defined as: γ_{obs} is the observed uptake coefficient, γ_t is the true uptake coefficient, the bulk density of the powder (ρ_b), the surface area of the samples (S_{BET}), the external and internal heights of the powder layers (h_e, h_i), and the effectiveness factor (η). The effectiveness factor is the ratio of the internal surface area that contributes to uptake of the gas molecules. The linear mass dependent (LMD) regime is a simpler method and generates comparable results to the KML model.[5] The LMD model uses the slope of the linear region of

observed uptake versus sample mass plots and multiplies it by the area of the sample holder (A_s) divided by the surface area of the sample (S_{BET}). (Equation 1.4)[5]

$$\gamma_t = \text{slope}\ (\text{mg}^{-1})\ \frac{A_S(\text{cm}^2)}{S_{BET}(\text{cm}^2\text{mg}^{-1})} \tag{1.4}$$

If the mass of the mineral dust sample is known to fall within the LMD regime, Equation 1.5[5] can be used in place of Equation 1.4.

$$\gamma_t = (\frac{A_s}{A_{BET}})\gamma_{obs} \tag{1.5}$$

Both models were used to determine the true uptake coefficients of VOCs by mineral oxides studied by Carlos-Cuellar et al.[5] and Li et al.[46]. The uptake coefficients are listed in Table 1.7.

Table 1.7 – True uptake coefficients calculated using either the KML or LMD models.[5,46]

	VOC		
Oxide	Acetic Acid	Methanol	Formaldehyde
SiO_2	$(2.4 \pm 0.4) \times 10^{-4}$	$(4 \pm 2) \times 10^{-6}$	$(2.6 \pm 0.9) \times 10^{-7}$
α-Al_2O_3	$(2 \pm 1) \times 10^{-3}$	$(1.0 \pm 0.7) \times 10^{-4}$	$(7.7 \pm 0.3) \times 10^{-5}$
α-Fe_2O_3	$(1.9 \pm 0.3) \times 10^{-3}$	$(1.9 \pm 0.4) \times 10^{-4}$	$(1.1 \pm 0.5) \times 10^{-4}$
	Acetaldehyde	Acetone	Propionaldehyde
SiO_2	7.0×10^{-6}	6.2×10^{-6}	1.1×10^{-5}
α-Al_2O_3	3.2×10^{-5}	2.0×10^{-5}	4.7×10^{-5}
α-Fe_2O_3	2.9×10^{-6}	1.6×10^{-4}	5.1×10^{-5}

The uptake coefficients listed in Table 1.7 can be used to infer how reactive the respective surface is toward each VOC. SiO_2 was found to have the smallest uptake coefficients in every case studied in these papers. The results of the Knudsen cell experiments combined with FTIR measurements of SiO_2 exposed to the various VOCs revealed each VOC weakly adsorbs to the SiO_2 surface. Terminal hydroxyl groups on the SiO_2 surface hydrogen bonded to the gas phase VOCs. FTIR confirmed the presence of the VOCs on the surfaces used in this study. For SiO_2, the uptake was observed to be reversible.[5,46] Unlike SiO_2, the uptake of these VOCs on α-Fe_2O_3 and α-Al_2O_3 were found to be irreversible. Acidic sites on these two oxides reacted with the VOCs, such as methanol and acetic acid, to produce surface adsorbed acetate

and methoxide ions.[5,46] SiO_2 showed no significant reactivity toward the VOCs studied here, but α-Fe_2O_3 and α-Al_2O_3 chemically reacted with the VOCs to produce surface adsorbed products.

Chen et al.[41] studied the reactions between VOCs adsorbed to the surface of SiO_2 and ozone. SiO_2 powder was pressed onto a stainless steel grid and mounted in an IR flow cell. Samples were exposed to methacrolein (MAC) or methyl vinyl ketone (MVK) and IR spectroscopy monitored the interaction between the VOCs and the SiO_2. Spectra showed that the adsorption mechanism of MVK and MAC on SiO_2 was dominated by hydrogen bonding. Upon evacuating the IR flow cell of MVK or MAC, the characteristic peaks of the VOCs on SiO_2 disappeared. Before the VOCs desorbed from the surface, ozone was introduced into the flow cell. Ozone reacted with the surface adsorbed MVK and MAC and produced formic acid, acetic acid, methylglyoxal, formaldehyde, and organic peroxides. Chen et al. showed in their study that adsorbed VOCs can react with gas phase oxidants to produce harmful organic compounds such as methylglyoxal. Mineral dust aerosols can react with a variety of compounds that are present in the atmosphere. The results of these reactions range from simple desorption of the compound, irreversible adsorption of products, and long range transport and reaction of adsorbed products with other atmospheric species.[41] More information is needed to determine the broader effects mineral dust aerosols have on atmospheric chemistry.

1.4. Future Experiments

Mineral dust aerosols introduced into the atmosphere have the potential to impact several aspects of atmospheric chemistry. It is important to study these effects in order to gain a broader understanding of the chemical processes occurring in the atmosphere. Knudsen cells are a proven method to study the kinetics of atmospherically relevant chemical pathways.

The following chapters describe the construction and testing of a Knudsen cell designed to study the kinetics of heterogeneous chemical reactions of atmospheric relevance. Details of the design of the cell are discussed in Chapter 2. The goal of these studies is to determine the uptake coefficient of gas phase species with solid surfaces. By measuring the uptake coefficient, we can theorize the importance of a specific heterogeneous reaction in the atmosphere. Our studies will focus on the uptake of VOCs on SiO_2, one of the most abundant crustal compounds.[13] Theses studies will not only provide new insight into reactions not previously studied, but will also validate the effectiveness of the new Knudsen cell. Three benchmark tests will be performed on the Knudsen cell. The first will measure the uptake of ethanol on a clean stainless steel sample disc. Second, the uptake of methanol on SiO_2 measured in our Knudsen cell will be compared to the work of Carlos-Cuellar et al.[5] to serve as a benchmark test for the instrument. The final study will test whether or not we can measure uptake coefficients proportional to surface areas of different samples. After the instrument is validated, we will measure the uptake of ethanol on SiO_2, which to our knowledge has not been previously done. The studies proposed here will validate the effectiveness of the new Knudsen cell as well as provide new insight into the uptake of ethanol on SiO_2.

1.5. Summary

Mineral dust aerosols can impact crucial atmospheric chemical processes, and the increasing amount of these aerosols in the atmosphere is cause for concern. Mineral dust aerosols absorb thermal radiation from the Earth's surface and either inhibit or promote cloud growth. Changes in cloud growth have an overall impact on the Earth's hydrological cycle. Mineral dust aerosols can react with atmospheric oxidants such as ozone, OH radicals, and NO_x species. These reactions can be significant sinks for these gas phase compounds.

Interactions between mineral dust aerosols and VOCs are of key interest to atmospheric studies. Mineral dust aerosols can transport adsorbed VOCs over long distances, and adsorbed VOCs can react with other atmospheric species. Loss of VOCs and atmospheric oxidants through the various pathways discussed previously can alter the chemistry of the atmosphere. Understanding how these processes change the overall chemistry of the atmosphere is of key interest to future studies. Future work will focus on the construction and testing of a new Knudsen cell to validate the instrument so it can be used to study reactions of atmospheric importance.

Chapter 2

Design of the Knudsen Cell and Experimental Approach

2.1. Introduction

Knudsen cell reactors use the gas phase property of effusion to study heterogeneous and homogeneous chemical pathways.[1,7,9,53] A typical Knudsen cell (Figure 2.1) consists of a sealed chamber that holds a sample with only a small opening for gas molecules to escape. Samples are covered while the chamber is filled with a gas species of interest through a leak valve attached to the chamber. Knudsen cells operate at pressures that fall into what is known as the "molecular flow" regime where gas phase collisions are minimized.[9,54] When pressure falls within the molecular flow regime, molecules flow through the aperture unhindered.[55] Once gas molecules escape the cell, they are analyzed by an analytical instrument (FTIR, mass spectrometry, etc.). When steady state conditions are achieved, the samples are uncovered and exposed to the gas, and changes in the flow of gas molecules escaping the chamber are measured. Changes in flow reveal kinetic information about reactions studied in the cell. This simple design has proved to be a robust tool to study homogeneous and heterogeneous chemical reactions.

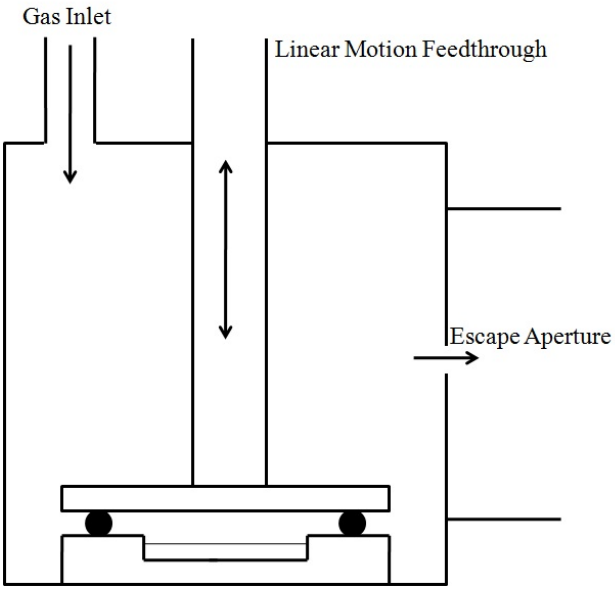

Figure 2.1 – Schematic of a simple Knudsen cell.

2.2. Background

A Knudsen cell was developed based on the work of Golden et al. for the purpose of studying heterogeneous reaction pathways of atmospheric importance.[7] Golden et al.[7] was the first to develop the Knudsen cell and demonstrate its effectiveness as a research tool. The Knudsen cell reactor, designed by Golden, operated at pressures in the millitorr range in order to operate in the molecular flow regime. During a typical experiment, Golden introduced a reactant gas and allowed the pressure to stabilize to a point where effusion occurred at the aperture. At this point, the sample was exposed and a mass spectrometer analyzed the escaping gas molecules.[7,9] The Knudsen cell developed by Golden et al. demonstrated one can study extremely fast homogeneous and heterogeneous chemical reactions at different temperatures as well as the energy transfer between molecules.[7] The technique presented by Golden et al. was used as a basis for the design of Knudsen cells by other research groups and the one described in detail herein.

Caloz et al.[53] and Grassian et al.[5,46] have both constructed Knudsen cells with the intent to study heterogeneous chemical reactions of atmospheric relevance. The cell designed by Caloz[53] consisted of a sample chamber and a differentially pumped chamber to house the mass spectrometer. (Figure 2.2) The small chamber was a combination of Teflon® coated stainless steel and glass. Teflon® minimized reactions between gas molecules of interest and the chamber walls. Viton® o-rings sealed the chamber off from atmospheric contaminants.

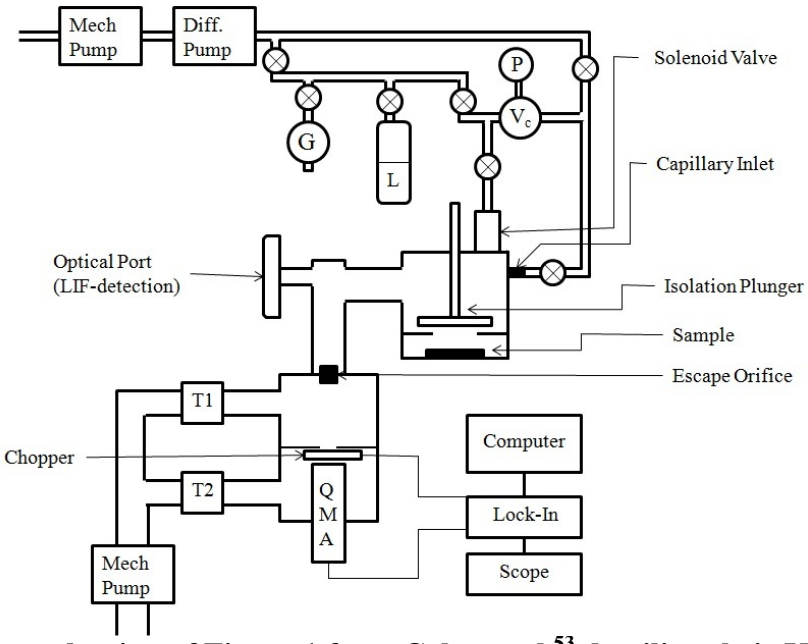

Figure 2.2 – Reproduction of Figure 1 from Caloz et al.[53] detailing their Knudsen cell design.

The gas manifold attached to the Knudsen cell was equipped to expose surfaces to gas (G) and liquid (L) vapors. A Baratron (P) monitored the pressure in the manifold. A section of the manifold was calibrated to a known volume (V_c) for mass flow calibrations. Two turbomolecular pumps (T1, T2) differentially pumped the mass spectrometer chamber. The chopper wheel in the mass spectrometer chamber modulated the effusive beam of molecules exiting the cell. The optical port in the main cell was utilized to employ spectroscopic techniques, such as Laser Induced Fluorescence (LIF), to analyze gas phase species in the

chamber.[53] Grassian et al.[5,46] developed a Knudsen cell, based on work done by Golden et al.[5,46] and Caloz et al.[53]

Grassian et al.[5,46] developed two different versions of a Knudsen cell. The first (Figure 2.3) was similar to Caloz's design, discussed previously.

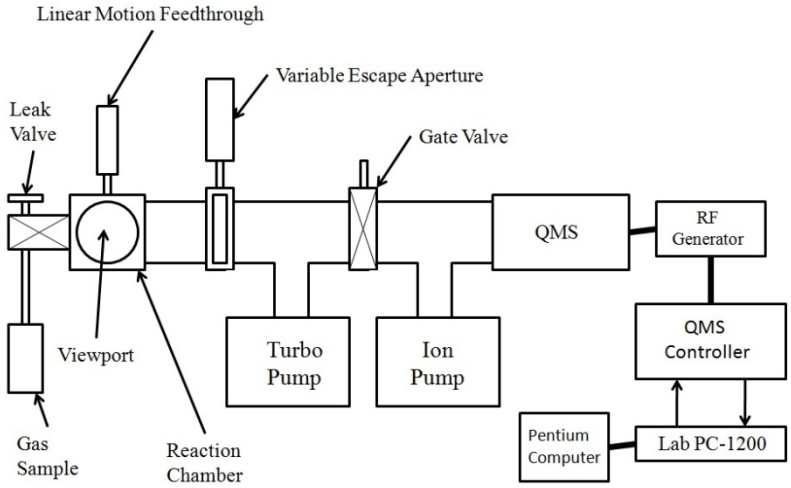

Figure 2.3 – Reproduction of Figure 1 from Grassian et al.[5] which shows one of the Knudsen cells designed by this group.

The cell consisted of a stainless steel reaction chamber to house the sample. A linear motion feedthrough with an o-ring lined cap on the end isolated the sample from the chamber atmosphere. A pumping differential created by the turbo pump in the mass spectrometer chamber increases the mean free path of the gas molecules exiting the reaction chamber. Mean free path is defined as the average distance a gas molecule can travel before it collides with another gas molecule.[56] For our studies, a large mean free path is needed for two reasons. First, a mean free path larger than the dimensions of the chamber minimizes gas phase collisions. Gas molecules only collide with the walls and the surface of the sample inside the chamber. Second, a large mean free path ensures molecules will travel unhindered from the reaction chamber to the mass spectrometer.[5] The Knudsen cell designed for our work is based off the work presented here and this group's experience with vacuum technology.

2.3. Knudsen Cell Design

The goal of the design of the Knudsen cell was to ensure that higher pressures in the uptake chamber during an experiment result in little to no change in pressure in the mass spectrometer chamber. Our design succeeded in accomplishing this goal. To demonstrate, consider a typical experiment where the chamber is sealed off. The conditions of this experiment are shown in Figure 2.4. For this example, the chamber is filled with ultra high purity (UHP) N_2 to a pressure of 1×10^{-4} Torr. This pressure is used to ensure a mean free path greater than the farthest distance, 22.6 cm, of the uptake chamber. Molecular flow is achieved at this pressure and the gas effuses through the first aperture into the differential chamber. Once the gas enters the differential chamber it passes through the second aperture into the mass spectrometer chamber.

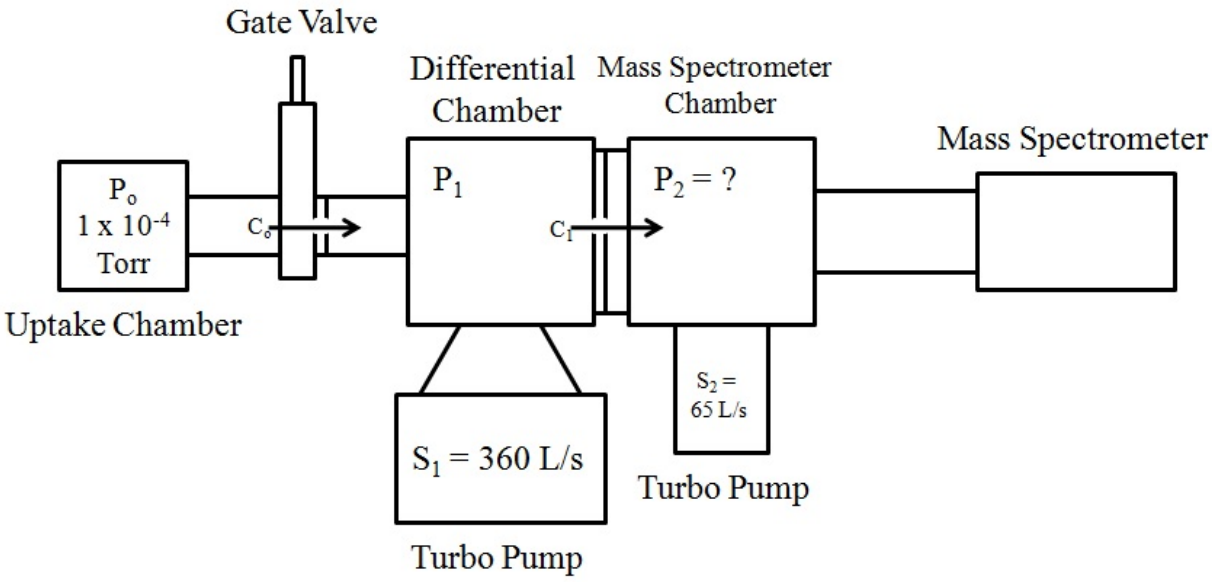

Figure 2.4 – Knudsen cell schematic detailing the conditions for the example described above.

The volume of gas that passes through the aperture per second is defined as conductance (C). Conductance (Equation 2.1) is equal to one quarter the product of the average velocity of the gas molecules ($\bar{\upsilon}$) flowing through the aperture with a defined area (A).

$$C = \frac{1}{4}\bar{\upsilon}A \quad (2.1)$$

With a diameter of 0.30 cm, the area of the two apertures is 0.0707 cm^2, and the average velocity of nitrogen at room temperature is 5×10^4 cm/s. The conductance of nitrogen through both apertures is calculated to be 884 cm^3/s or 0.884 L/s. The conductance of gas molecules through an aperture is related to the pressure in the chamber by using throughput.

Throughput (Q) is defined as the amount of gas that passes through a plane at any given time.[56] The pressure must be known to accurately calculate the amount of gas. As nitrogen enters the differential chamber, the throughput into the differential chamber equals the pressure of the uptake chamber (P_o) multiplied by the conductance of nitrogen through the first aperture (C_o). The throughput out of the differential chamber equals the pressure in the differential chamber (P_1) times the pumping speed (S_1) of the pump attached to this chamber. Under steady state operations, throughput into a chamber is equal to throughput out of the chamber. (Equations 2.2 and 2.3)

$$Q_{in} = Q_{out} \quad (2.2)$$
$$P_o C_o = P_1 S_1 \quad (2.3)$$

However, the effusive beam of nitrogen that exits the uptake chamber will pass through the differential chamber and enter the mass spectrometer chamber. The throughput into the mass spectrometer chamber is equal to the pressure of the differential chamber multiplied by the conductance (C_1) through the second aperture. Throughput of the gas out of the mass spectrometer chamber equals the pressure in the mass spectrometer chamber (P_2) times the pumping speed (S_2) of the pump attached to the mass spectrometer chamber. (Equations 2.4 and 2.5)

$$Q_{in} = Q_{out} \quad (2.4)$$
$$P_1 C_1 = P_2 S_2 \quad (2.5)$$

By combining the throughput equations (2.3 and 2.5), Equation 2.6 defines the relationship of pressure in the uptake chamber and pressure in the mass spectrometer chamber.

$$P_2 = \frac{P_o C_o C_1}{S_1 S_2} \tag{2.6}$$

Using Equation 2.6, one can calculate the pressure of the mass spectrometer chamber based on the pressure in the uptake chamber. Defining each value as follows: $P_o = 1 \times 10^{-4}$ Torr, C_o = 0.884 L/s, C_1 = 0.884 L/s, S_1 = 360 L/s, and S_2 = 65 l/s. The pressure in the mass spectrometer chamber (P_2) is equal to 3.34×10^{-9} Torr. The above example shows how the pumping differential allows for the pressure in the uptake chamber to be high while keeping the mass spectrometer chamber pressure in the low 10^{-9} Torr.

The main reason we need the pumping differential is to be able to optimally operate the mass spectrometer. If the entire chamber was brought up to a high dosing pressure, more than 10^{-4} Torr, the mass spectrometer would not function properly. The mass spectrometer's optimal operating pressures are 10^{-4} Torr for operation of the faraday cup and 10^{-6} Torr for operation of the electron multiplier. Without differential pumping, we could not operate the electron multiplier to enhance the signal to noise ratio to obtain adequate spectra for the studies completed for this work. By setting up the chamber with the series of apertures previously shown, the pressure in the mass spectrometer chamber is relatively unchanged by large increases in pressure in the uptake chamber. With the pumping differential in place, the mass spectrometer will operate optimally to ensure adequate data collection during the experiments carried out in the Knudsen cell.

Based on the design proposed for the above example, the Knudsen cell is constructed with the components detailed below. The uptake chamber (MDC Vacuum Products Corp.®, 665082) connects to the rest of the instrument with a manual elastomer sealed gate valve

(Huntington Mechanical Laboratories, Inc.®, GVA-150-V). The gate valve enables the researcher to isolate the uptake chamber from the rest of the instrument. The manual gate valve attaches to the first aperture (EMS Machine Shop, Diameter = 0.30 cm) of this set up. (Figure 2.5) Two six-way cubes (Kurt J. Lesker® Company, CU6-0450) comprise the mass spectrometer and differential chamber. Separating the two chambers is another aperture (EMS Machine Shop, Diameter = 0.30 cm) and a 4 ½" Multi-CF Close Coupler (Kimball Physics Inc.®, MCF450-CC20000-1400-A). A maximum insertion nipple with 4 ½" flange (MDC Vacuum Products Corp.®, 402004) mounts the mass spectrometer (Stanford Research Systems®, RGA 300/13) to the chamber. The nipple ensures the mass spectrometer filament is in a position for the best possible signal to noise ratio.

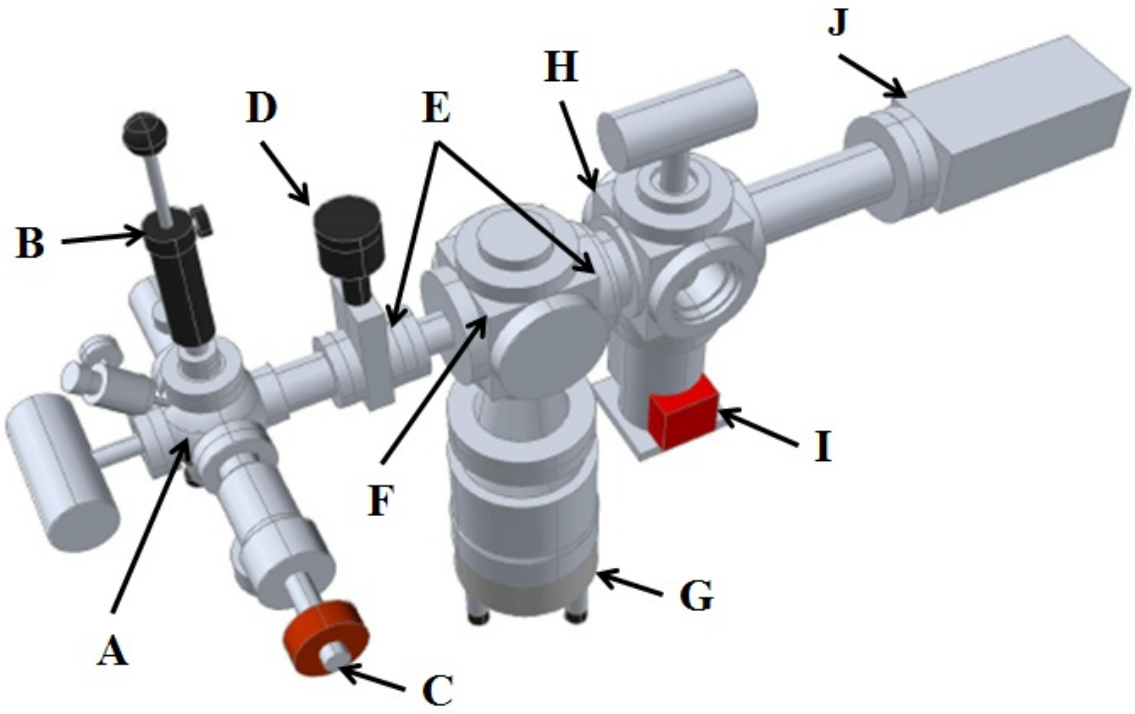

Figure 2.5 – Knudsen cell described in Chapter 2. Drawing rendered by AutoCAD®. Labeled parts are: (A) uptake chamber, (B) linear motion feedthrough, (C) right angle valve, (D) gate valve, (E) apertures, (F) differential chamber, (G) turbomolecular pump, (H) mass spectrometer chamber, (I) turbo drag pump, (J) residual gas analyzer (RGA)

A series of pumps maintains pressure in the Knudsen cell. HiCube™ 80 Eco pumping stations (Pfeiffer Vacuum®, PM S03 556) pump down the uptake and mass spectrometer chambers. A turbo drag pump, attached to each pumping station, maintains a pumping speed of 65 L/s. A turbomolecular pump (Oerlikon Leybold, TURBOVAC® 360) pumps on the differential chamber with a pumping speed of 360 l/s.[57] A scroll vacuum pump (Ideal Vacuum Products, P101948) backs the two turbo pumps on the uptake and differential chambers at a speed of 2.5 L/s. A diaphragm pump, housed in the HiCube™ Eco 80 pumping station, backs the turbo drag pump on the mass spectrometer chamber at a speed of .25 L/s. The pumping speeds ensure the pumping differential and adequate pressures are maintained in the Knudsen cell.

The key aspect of a Knudsen cell is the pressure in the cell falling within the molecular flow regime. Once molecular flow is obtained, the mean free path is greater than the dimensions of the chamber, which ensures collisions between individual molecules are minimized. The bulk of the collisions within the chamber are between the molecules and the walls of the chamber. Gas molecules can only exit the chamber by passing through the aperture and entering the differential chamber. By maintaining molecular flow in the chamber and only allowing molecules to exit via the aperture, the instrument qualifies as a Knudsen cell. Each chamber is designed with a specific purpose to complete a robust instrument to further compliment the research already completed in this group.

2.3.1. Uptake Chamber

The uptake chamber, the heart of the Knudsen cell, is equipped with several tools to contain and expose the samples to reactant gases. Seals on the stainless steel chamber (Figure 2.6) and the rest of the instrument are made with ConFlat™ (CF) flanges. CF flanges use a sharp

knife edge to cut into a copper gasket to form the seal. The six CF ports on the uptake chamber are attached to the ion gauge, right angle valve, two leak valves, linear motion feedthrough, and the last connects the uptake chamber to the gate valve.

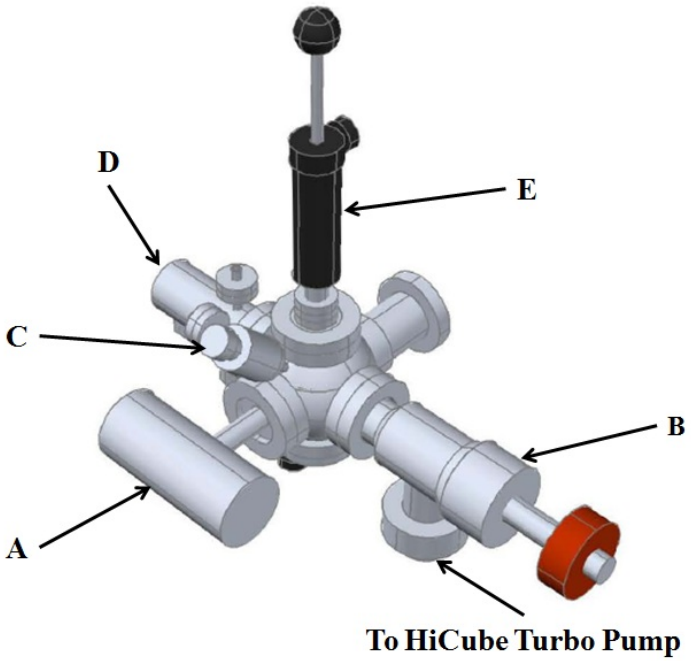

Figure 2.6 – Uptake chamber of the Knudsen Cell. The labeled parts are: (A) Beyard-Alpert ion gauge, (B) right angle valve, (C) variable leak valve, (D) variable leak valve, (E) linear motion feedthrough.

A Beyard-Alpert ion gauge (Kurt J. Lesker®, G075F) monitors pressure in the uptake chamber. Ion gauges measure pressure by flowing a current through a wire, which ionizes any gas molecules that collide with it. An internal grid collects the ions, and the positive ion current is converted to a pressure measurement.[56] The HiCube™ 80 Eco pumping station (not shown in Figure 2.6) attaches to the chamber by way of a right angle valve (Huntington Vacuum, MV-150) and maintains high vacuum pressures in the uptake chamber. The right angle valve isolates the chamber from the turbo pump during an experiment so the gas molecules only escape through the aperture into the differential chamber. When the chamber is isolated, there are two ways to introduce gases of interest. The first is a Variable Leak Valve (MDC Vacuum Products

Corp.®, 315002) attached to the uptake chamber by a mini CF flange (1.33 in OD). A mini CF flange with a Swagelok® adapter allows us to connect a custom glass bulb, with a glass to metal connection, to the chamber. Connections are made with stainless steel tubing between the Swagelok® adapter and a stainless steel ¼" union. Attached to the Swagelok® union is the custom glass bulb filled with the volatile organic compound (VOC) of interest. Another method for introducing gas into the chamber is through a second leak valve (MDC Vacuum Products Corp.®, 315010) connected to one of the CF ports of the chamber. A second mini flange to ¼" Swagelok® adapter is attached to the leak valve. Using several pieces of stainless steel tubing, a ¼" Swagelok® T connection (Swagelok®, SS-400-3) and two Swagelok® Bellows Sealed Valves (SS-4H), a small manifold is constructed. (Figure 2.7) A glass bulb can be attached to each valve, which allows for the dosing of up to two gases at once.

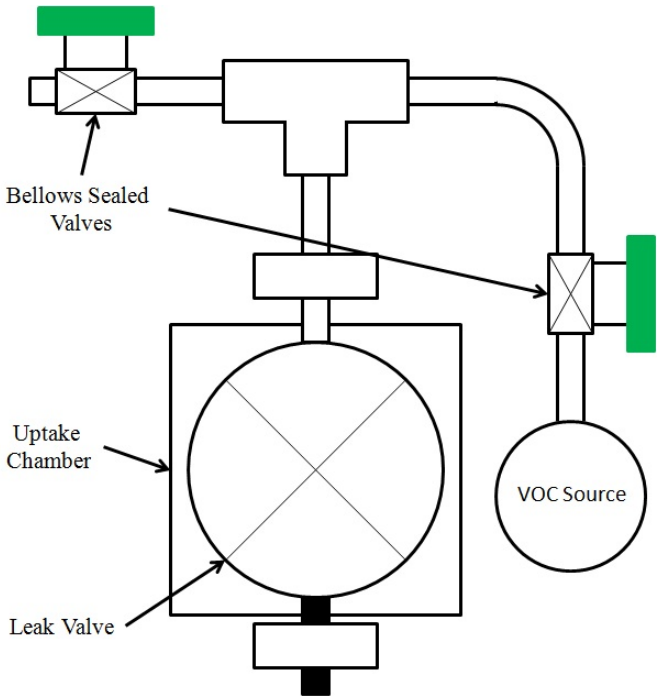

Figure 2.7 – Gas manifold attached to the uptake chamber.

The final port on the uptake chamber is devoted to a linear motion feedthrough (MDC Vacuum Products Corp.®, 663004). A linear motion feedthrough consists of a stainless steel

actuator, which extends into the uptake chamber. The part is constructed with a position lock, which allows for control over the exact position of the cap attached to the end of the feedthrough. The stainless steel cap on the end of the feedthrough is lined with a Viton® o-ring (Figure 2.8) for the purpose of isolating a sample from the rest of the chamber environment during an experiment. The linear motion feedthrough plays an important role in the experimental process to be discussed later. The uptake chamber is equipped with the capabilities to dose surfaces with more than one reactive gas, and the sealed chamber only allows gases to escape through the aperture into the differential chamber.

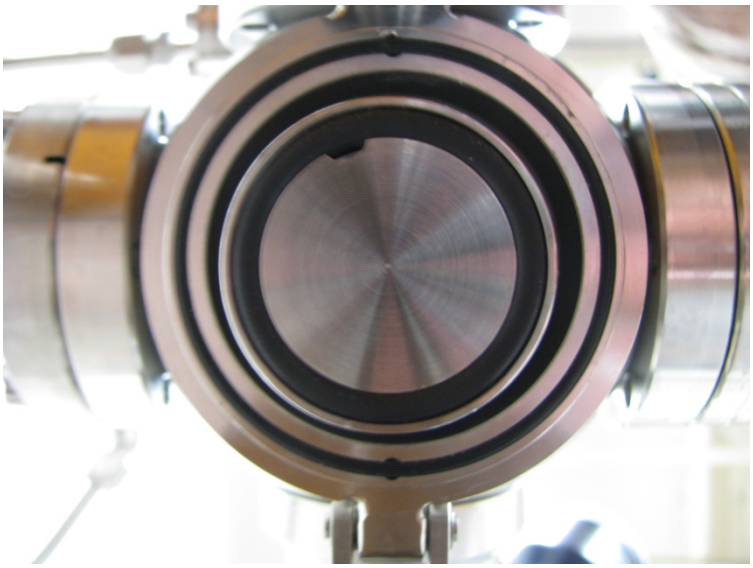

Figure 2.8 – View of the linear motion feedthrough cap from the bottom up.

2.3.2. Differential Chamber

The differential chamber (Figure 2.9) connects to the uptake chamber by way of a straight tube nipple reducer from a 4 ½" outer diameter (OD) flange to a 2 ¾"OD flange (MDC Vacuum Products Corp.®, 402013). The six-way cube making up this chamber has six 4 ½" flange connections, one is used to connect the chamber to the uptake chamber. One side port is blanked off with a 4 ½" OD blank CF flange (Kurt J. Lesker® Company, F0450X000N), and the other side is sealed with a 4 ½" OD CF zero length kodial glass viewport (Kurt J. Lesker ®

Company, VPLZ-450). The turbomolecular pump attaches to the bottom port of the cube via a 6" OD to 4 ½" OD CF conical reducer (Kurt J. Lesker® Company, CRN600x450). The fifth port, the top port of the six-way cube, is sealed with a 4 ½" OD to 2 ¾" OD zero length reducing CF flange (Kurt J. Lesker® Company, RF450X275). The reason for using this type of flange is for the option to attach another gauge to monitor pressure or some other apparatus to the cell in the future. The low pressures maintained in the differential chamber minimize gas phase collisions for molecules exiting the uptake chamber. Gas molecules continue unhindered through the second aperture, attached to the final port of the cube, and a 4 ½" Multi-CF Close Coupler into the mass spectrometer chamber.

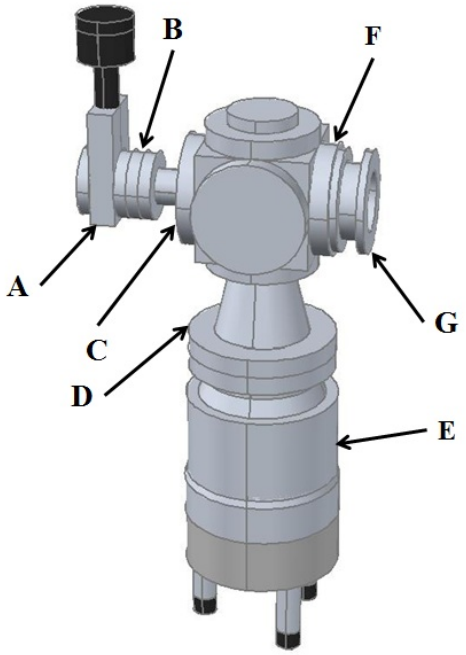

Figure 2.9 – Differential chamber of the Knudsen cell. Labeled parts are: (A) manual gate valve, (B) aperture, (C) reducing flange, (D) conical reducer, (E) turbomolecular pump, (F) aperture, (G) close coupler

2.3.3. Mass Spectrometer Chamber

Similar to the differential chamber, a six way cube makes up the mass spectrometer chamber (Figure 2.10). The turbo drag pump from the HiCube™ 80 Eco pumping station

attaches to the base of the cube. 4 ½" OD blank CF flange and a 4 ½" OD CF zero length kodial glass viewport seals the side ports of the cube. A second ion gauge (Kurt J. Lesker®, G100F) is mounted to the top port of the six-way cube with a 4 ½" OD to 2 ¾" OD zero length reducing CF flange. Pressure stabilizes in the low to mid 10^{-9} Torr during an experiment and can reach pressures in the high 10^{-10} Torr. The maximum insertion nipple (MDC Vacuum Products Corp.®, 402004) attaches the mass spectrometer to the six way cube so the filament is just inside the chamber. The mass spectrometer attached to the chamber is a residual gas analyzer (RGA), which is a simple quadrupole mass spectrometer (Stanford Research Systems®, RGA 300/13). The RGA used on this chamber can scan masses over a range of 1 to 300 amu with adequate resolution for the studies performed and discussed in Chapter 3.

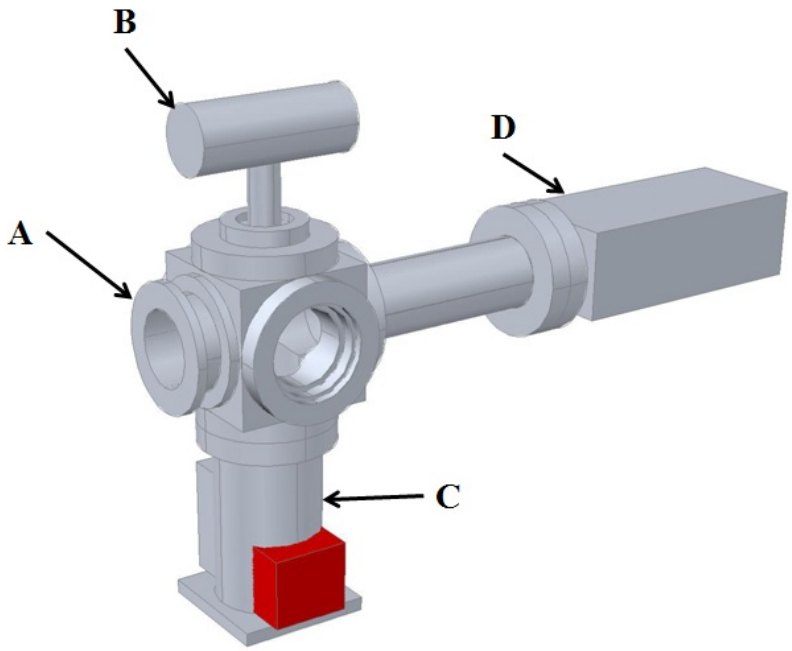

Figure 2.10 – Mass spectrometer chamber. Labeled parts are: (A) close coupler, (B) Beyard-Alpert ion gauge, (C) turbo drag pump, (D) residual gas analyzer (RGA)

2.3.4. System Overview

The Knudsen cell is a robust experimental instrument designed to study a wide range of concepts not previously studied by this group. Not only will this instrument open new research

pathways, it will also allow for the expansion of research available to past projects. Using up-to-date vacuum techniques the chamber maintains pressure from 10^{-6} Torr in the uptake chamber to 10^{-10} Torr in the mass spectrometer chamber. The three stainless steel chambers, which make up the Knudsen cell, are equipped to study heterogeneous reactions that bear significance to chemistry occurring in the atmosphere. The first test of the Knudsen cell will study the uptake of VOCs on a silica surface.

2.4. Experimental Procedure

2.4.1. Volatile Organic Compound Preparation

A VOC source must be properly purified of any residual gases before it can be used in a dosing experiment inside the Knudsen cell. To introduce VOCs into the chamber, clean glass bulbs with metal to glass connections are outfitted with ¼" Swagelok® nut and ferrules and filled with 3-5 mL of the VOC of interest. The filled glass bulb is attached to one of the leak valves on the uptake chamber. The VOC is purified with the freeze, pump, and thaw method. Submersing the bulb in a cup of liquid nitrogen freezes the VOC. Once the VOC freezes, gases in the bulb are pumped out by the turbo drag pump attached to the uptake chamber. The ion gauge on the uptake chamber and the RGA monitor pressure and content of the gas molecules in the uptake chamber respectively. Once the chamber has pumped down and the RGA shows typical levels of trace gases in the chamber, the bulb is allowed to thaw with the liquid nitrogen removed. Isolating the bulb from the pump when the VOC begins to appear in the mass spectrum completes one cycle of the freeze, pump, and thaw method. Once thawed, any residual gas dissolved into the VOC will fill the bulb and the cycle is repeated at least three times. After purifying the VOC, it can be used in a dosing experiment.

2.4.2. Sample Preparation and Loading into the Chamber

Samples loaded into the chamber are placed in custom-made stainless steel discs (Figure 2.11). The discs are made to have a slip fit with a depression cut into the door of the uptake chamber.

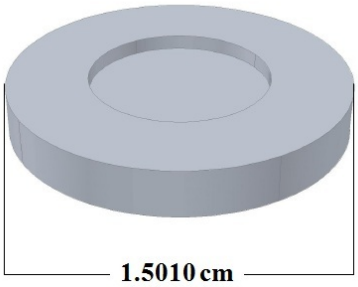

Figure 2.11 – Stainless steel sample holder.

Silica gel (Aldrich®, 200-400 mesh, BET = 500 m^2/g) is used as the SiO_2 surface for these experiments. Silica gel samples are weighed out and spread across the sample disc. Pressing the samples manually with gentle pressure forms a level surface. Pressed samples are loaded into the chamber and carefully pumped down to keep the sample intact.

Loading a sample into the chamber involves opening certain valves while keeping others closed in order to only vent the uptake chamber while the differential and mass spectrometer chambers remain pumped down. First, closing the gate valve isolates the uptake chamber from the rest of the system. The turbo drag pump is turned off and isolated from the scroll pump by closing the uptake foreline.

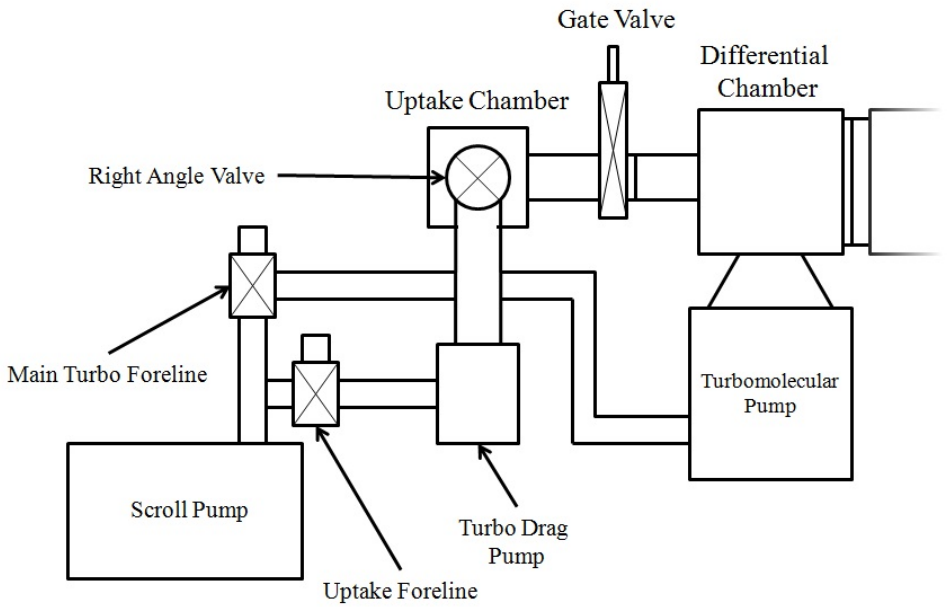

Figure 2.12 – Detail of pumps involved in venting and pumping down the uptake chamber during sample transfer.

After the pump has spun down, the uptake chamber vents by opening a small black knob on the back of the turbo drag pump. Closing this black knob occurs after the chamber has vented and before the system is pumped down again. Double sided tape secures the sample disc to the door of the uptake chamber. Since the sample door hangs freely below the chamber, the door must be held closed during the initial pump down to ensure an adequate seal. Before the pump down of the uptake chamber begins, the turbomolecular pump on the differential chamber must be isolated from the scroll pump. Failure to isolate the turbomolecular pump causes a large pressure spike in the differential and mass spectrometer chambers during the initial pump down of the uptake chamber. The spike in pressure occurs when gas from the uptake chamber travels up the main turbo foreline. With the turbomolecular pump isolated, the uptake foreline is opened slowly to decrease the chances of disturbing the sample. After the turbo drag pump spins up to 1500 Hz, the current of the pump indicates the quality of the seals in the chamber. If the current falls within a range of 0.14 – 0.10 A, the chamber seals are sufficient and the pump down continues. Once the pressures reaches 10^{-6} Torr, the gate valve is opened between the uptake and

differential chambers. An overnight pump down, 12 – 15 hr., removes a majority of atmospheric contaminants, such as nitrogen and water, adsorbed on the wall of the chamber and the silica sample. Removal of these contaminants reduces the effect they will have on uptake measurements obtained during surface exposure.

2.4.3. Exposing a Sample to Volatile Organic Compounds

After the sample pumps down overnight, the Knudsen cell can measure the uptake coefficients of VOCs on silica. To start the experiment, the linear motion feedthrough is lowered over the sample so that it is sealed off from the chamber atmosphere. (Figure 2.13)

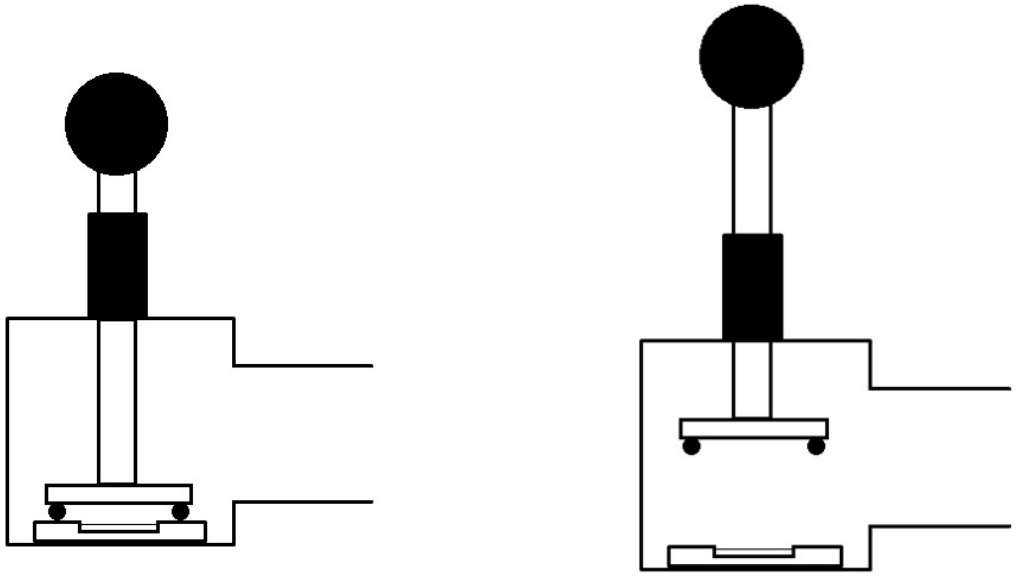

Closed **Open**

Figure 2.13 – The two stages of the linear motion feedthrough during an experiment.

Closing the right angle valve seals the uptake chamber from the attached turbo drag pump and makes it so only gas molecules escape through the first aperture. After sealing the chamber, the pressure rises by slowly leaking the VOC into the cell. For these experiments to work the pressure in the uptake chamber must ensure the mean free path (λ) of the VOC is greater than the dimensions of the chamber. At this pressure, gas phase collisions between molecules are

minimized. Mean free path (Equation 2.7) is equal to 1 divided by the product of the square root of two, pi (π), the number density (n = molecules/m^3), and diameter of the molecule (d = m).[56]

$$\lambda = \frac{1}{2^{1/2}\pi n d^2} \tag{2.7}$$

The greatest distance gas molecules travel in the uptake chamber is 22.6 cm. Using a mean free path of 25 cm and solving Equation 2.7 for n, the number density needed to achieve this mean free path can be calculated. (Equation 2.8)

$$\mathrm{n} = \frac{1}{2^{1/2}\pi \lambda \mathrm{d}^2} \tag{2.8}$$

The number density calculated to achieve a mean free path of 25 cm for ethanol is 5.67×10^{18} molecules/m^3. The pressure required to achieve the needed number density is calculated using the ideal gas law. For a mean free path of 25 cm, the Knudsen cell must be at a pressure of 1.7×10^{-4} Torr. The pressure in the mass spectrometer chamber determines the pressure in the uptake chamber using Equation 2.6, because the ion gauge on the uptake chamber can act as a reactive surface it is left off during an experiment. When the pressure reaches 3.1×10^{-9} Torr in the mass spectrometer chamber, the pressure in the uptake chamber has reached 1.7×10^{-4} Torr. Once the pressure equilibrates, sample exposure begins by raising the linear motion feedthrough cap up off the sample. Samples are exposed for seven minutes after which the reactive gas flow stops. The uptake chamber pumps down for one hour before the next exposure.

2.4.4. Data Acquisition

The only analytical tool currently attached to the Knudsen cell is a mass spectrometer, a residual gas analyzer (RGA). Scans are taken with the RGA at the very beginning of the experiment and are focused around the base peak of the VOCs used. For ethanol, scans are taken in a range from 29 – 33 amu, since the base peak for ethanol is 31 amu due to a loss of a methyl

group.[58] Scans are compiled into a log and later converted into a mass spectrometer signal vs. time graph. From this data the uptake of certain VOCs can be determined for our samples.

2.5. Summary

A Knudsen cell, which utilizes molecular effusion, is an ideal tool for studying the kinetics of heterogeneous reactions. For the reason of expanding the scope of research done by this group, a Knudsen cell was designed and constructed. The system is designed so that the uptake chamber is isolated from its turbo drag pump during an experiment, so the only way for gas to escape is through the aperture to the mass spectrometer. By sampling the gas escaping from the chamber, without the presence of a reactive surface and with the presence of a reactive surface, the reactive uptake of the gas on a surface can be determined. The first system studied with this instrument is the uptake of ethanol on silicon dioxide, a mineral dust aerosol present in the atmosphere. The goal of the study is to validate the newly built Knudsen cell and learn more about the chemistry occurring between VOCs and SiO_2.

Chapter 3

Performance Evaluation of a Knudsen Cell Reactor: Uptake of Ethanol on Silicon Dioxide

3.1. Introduction

Silicon is one of the most abundant crustal elements, and silicon dioxide (SiO_2) in the form of quartz is one of the most common mineral dust aerosols.[13] 800 – 2000 Tg of mineral dust aerosols are emitted each year into the atmosphere.[1,4,11] SiO_2 can be transported over large distances and serve as a reactive sink for important atmospheric species. Compounds adsorbed on the surface of SiO_2 can be carried over long distances before the compounds desorb from the surface or react with other atmospheric species.[5,6,10,11,41] Previous studies of reactions involving SiO_2 show the compound is not as reactive as other mineral dust aerosols, but because of its prevalence in the atmosphere, it is an important surface to study.

The reactive uptake of VOCs, methanol, acetone, acetaldehyde, and formaldehyde, on SiO_2 has been studied previously.[5,46] VOCs are introduced into the atmosphere by way of biomass burning, incomplete fuel combustion, and the use of organic solvents in industry. The amount of VOCs introduced into the atmosphere a year are comparable to the amount of mineral dust aerosol emissions.[3,39] The work presented here studies the reactions of the VOCs, methanol and ethanol, with SiO_2. The goal of this work is to evaluate the effectiveness of the Knudsen cell (Chapter 2) and to provide new insight into the uptake probability of VOCs on SiO_2.

The evaluation of the Knudsen cell's effectiveness consists of three separate studies. The first, measures the uptake of ethanol on a clean sample holder with no SiO_2. Without the presence of SiO_2 the observed uptake of ethanol on the sample holder is expected to be zero. The uptake of methanol is measured on SiO_2 and compared to the work done by Carlos-Cuellar

et al.[5] Observed uptake of methanol on SiO_2 in our chamber is expected to be within one order of magnitude of Carlos-Cuellar et al work. The final test of the effectiveness of the Knudsen cell measures the uptake of ethanol on two samples of activated charcoal with known surface areas. Observed uptake measured in this third test is expected to be proportional to the surface area of both samples. After establishing the effectiveness of the Knudsen cell, the uptake of ethanol on SiO_2 is measured. To our knowledge, we present one of the first studies of ethanol uptake on SiO_2.

3.2. Experimental

3.2.1. Sample Preparation

Samples of silica gel (Aldrich®, 200-400 mesh, Surface Area = 500 m^2/g) and two different types of activated charcoal (Aldrich®, 8 – 20 mesh, Surface Area = 600 – 800 m^2/g; Aldrich, 100 – 400 mesh, Surface Area = 1400 m^2/g) were used as purchased. The silica gel served as the SiO_2 surface in the uptake studies involving methanol and ethanol. Silica gel was spread across the sample discs. (Figure 2.11) For the methanol studies, a single mass of 16.0 mg was used, and for the ethanol studies the samples masses ranged from 7 – 100 mg. The samples were pressed manually to achieve as smooth a surface as possible. Next, the samples were loaded into the uptake chamber following the method detailed in Chapter 2. The two types of activated charcoal were prepared two different ways for the surface area studies. Activated charcoal with a surface area of 600 – 800 m^2/g was granular. It could not be pressed into the sample disc, and only small granules were used because the inner depression of the disc is shallow. The inner depression was packed as tightly as possible with the charcoal granules. The other charcoal sample with a surface area of 1400 m^2/g was prepared the same way as the silica samples. The same mass used for both charcoal samples.

3.2.2. Volatile Organic Compound Preparation

Ethanol (Decon Laboratories, Inc.) and methanol (Fisher Scientific) were purified before use in the Knudsen cell. 3-5 mL of the liquid was poured into a clean custom glass bulb outfitted with stainless steel Swagelok® connections to attach the bulb to one of the leak valves on the chamber. The ethanol and methanol were purified with freeze/pump/thaw cycles before it was used in experiments. The liquid in the glass bulb was frozen by submersing the bulb in a cup of liquid nitrogen. Once the liquid was frozen, the turbo drag pump on the uptake chamber pumped down the bulb after opening the leak valve to the pump. After the mass spectrometer showed normal levels of gases in the chamber, the bulb was raised out of the liquid nitrogen. The bulb was continually pumped as it thawed. When the liquid vapors began to appear in the mass spectrometer, the bulb was isolated from the pump. After the liquid has thawed, the cycle was repeated at least three times until the mass spectrometer spectrum showed minimal amounts of gas phase contaminants. Three freeze/pump/thaw cycles were enough to thoroughly purify the liquids for dosing.

3.2.3. Sample Exposure

To begin an experiment, the sample was isolated from the uptake chamber atmosphere by lowering the linear motion feedthrough cap over the sample. (Figure 2.13) The uptake chamber was sealed by closing the right angle valve so the gas can only escape through the aperture. Before the liquid vapor was introduced, the mass spectrometer scans the gases escaping the uptake chamber. The experimental steps outlined below are shown in Figure 3.1.

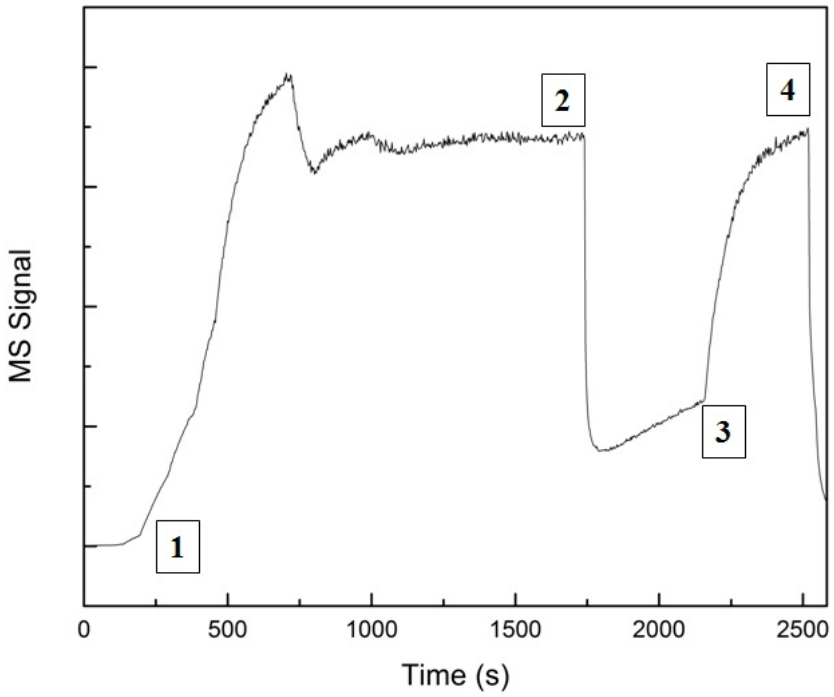

Figure 3.1 – Mass spectrometer signal vs. time graph of an ethanol uptake experiment on activated charcoal. The graph shows the different steps of a typical experiment. 1) The liquid sample is introduced into the uptake chamber. 2) After achieving steady state conditions, the sample is exposed for seven minutes. 3) The sample is covered and the signal recovers. 4) The liquid sample flow stops and the uptake chamber is pumped down.

One minute after the scan started (1), the uptake chamber was filled with the vapor of methanol or ethanol to obtain the pressure calculated in Chapter 2 for optimum experimental conditions. After the signal stabilizes in 28 min, sample exposure occurred by raising the linear motion feedthrough (2). The samples were exposed for seven minutes at which point the ethanol flow was stopped, but for this example the linear motion feedthrough was lowered back over the sample(3). Once the signal recovered and stabilized, the flow of ethanol was stopped. These experimental steps were followed for each sample studied here.

3.3. Results and Discussion

3.3.1. Mass Spectrometer Data

The uptake coefficients for each system studied was determined using the data from just before step 2 in Figure 3.1 to step 3, after the seven minute exposure. Figure 3.2 shows mass spectrometer (MS) data gathered during the seven minute surface exposure.

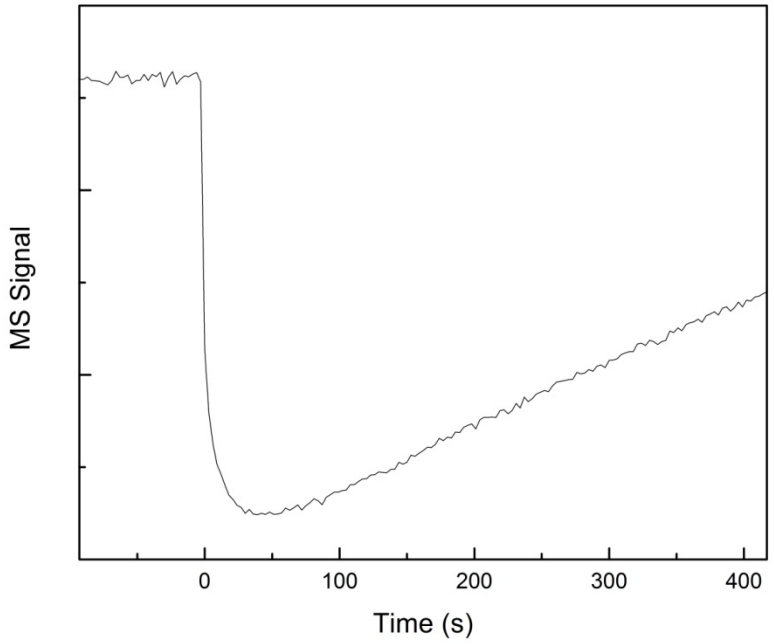

Figure 3.2 – Mass spectrometric data of ethanol loss on a silica gel surface. Only a short amount time before the seven minute exposure is shown. Surface was exposed at time 0 s.

The mass spectrometer was focused around the base peak for ethanol and methanol to obtain the data in Figure 3.2. The base peak for both ethanol and methanol was found to be 31 amu due to the ionization of each compound.[58] Ionization of ethanol resulted in the cleaving of a methyl (CH_3-) group and the loss of a hydrogen atom for methanol. The alcohol molecules were lost to the surface as indicated by the sudden drop in signal. As the surface became saturated with the alcohol, the signal began to recover gradually for the remainder of the exposure time. The initial drop and recovery time of the MS signal was dependent on the type of surface, the sample mass,

and the surface area of the individual particles.[5,30,40,46,50] For example, Figure 3.3 shows two plots of MS signal intensity vs. time for two samples of SiO_2 with ethanol. The red line is the MS intensity for the 99.1 mg sample and the blue line is the MS intensity for the 7.6 mg sample.

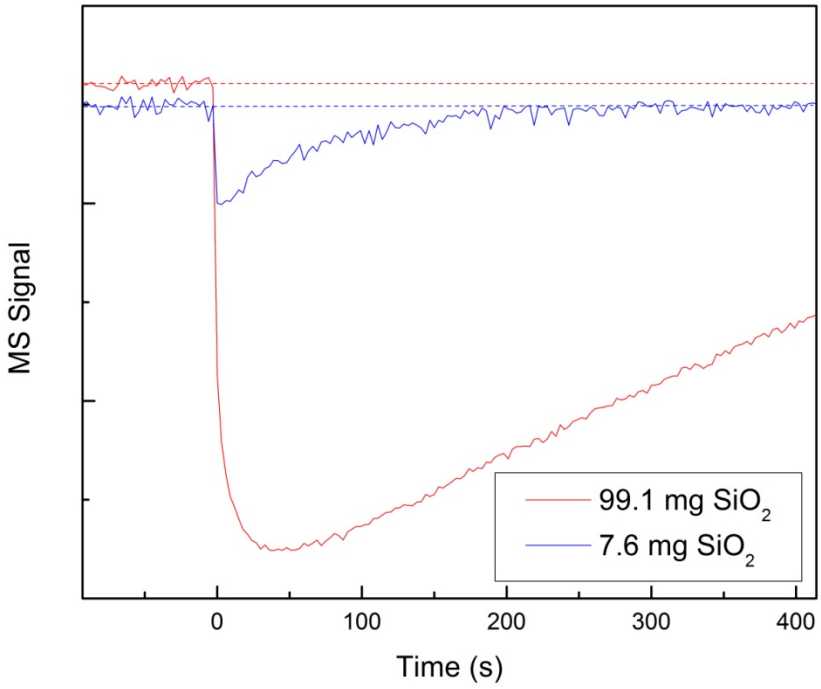

Figure 3.3 – Mass spectrometer signal vs. time plots of two SiO_2 samples: (Red) 99.1 mg and (Blue) 7.6 mg. Surfaces were exposed at time 0 s.

There are dramatic differences between the two plots. The initial drop in signal for the 7.6 mg sample was not as intense as the 99.1 mg sample due to the difference in sample mass, and within approximately five minutes after exposure the signal recovered to the original base line. The signal recovery increased for the 7.6 mg sample because there was a smaller surface area for the ethanol to saturate. Using the mass spectrometer data collected, the uptake coefficients of ethanol/methanol on SiO_2 were determined.

3.3.2. Uptake Measurements

The mass spectrometer data gathered for each sample can be used to determine the observed uptake coefficient (γ_{obs}) of ethanol on the surfaces studied. To accurately determine the uptake coefficient within the Knudsen cell, the surface area of the samples needed to be known, because the uptake coefficient is the loss of gas per surface area of the samples.[8] Equation 3.1 defines γ_{obs} as the loss of molecules from the gas phase per second divided by the gas surface collisions per second.[5,8]

$$\gamma_{obs} = \frac{loss\ of\ molecules\ from\ the\ gas\ phase\ per\ second}{gas{-}surface\ collisions\ per\ second} \tag{3.1}$$

The numerator of Equation 3.1 can be defined as $F_o - F$ where F_o is the flux of gas molecules out of the cell without a reactive surface and F is the flux in the presence of a reactive surface.[5,8] In the systems studied, gas molecules collide with a reactive surface site and are effectively "lost" to the surface either through adsorption, physisorption, and/or a reaction. The denominator of Equation 3.1 is defined as the gas-surface collision frequency (ω = col/sec), Equation 3.2.[8]

$$\omega = \tfrac{1}{4}\bar{\upsilon}A_s n \tag{3.2}$$

The collision frequency equation is ¼ the product of the average velocity of the gas molecules ($\bar{\upsilon}$), the geometric surface area of the sample (A_s), and the number density (n) of the gas molecules in the Knudsen cell.[8] Number density of the reactant gas in the Knudsen cell is related to flux of reactive gas molecules through the escape aperture of the cell. (Equation 3.3)[8]

$$n = \frac{4F}{A_h\bar{\upsilon}} \tag{3.3}$$

A_h in this equation is the area of the escape aperture of the Knudsen cell. Combining Equations 3.1 – 3.3 defines the uptake coefficient as what is seen in Equation 3.4.[5,8]

$$\gamma_{obs} = \frac{F_o - F}{\frac{\bar{\upsilon} A_s n}{4}}$$

$$\gamma_{obs} = \frac{F_o - F}{\frac{4\bar{\upsilon} A_s F}{4A_h \bar{\upsilon}}}$$

$$\gamma_{obs} = \frac{F_o - F}{\frac{4\cancel{\bar{\upsilon}} A_s F}{4A_h \cancel{\bar{\upsilon}}}}$$

$$\gamma_{obs} = \frac{A_h}{A_s}\left(\frac{F_o - F}{F}\right) \tag{3.4}$$

The flux of gas molecules out of the cell is directly proportional to the mass spectrometer signal (I), and with this relationship in mind, Equation 3.4 can be redefined to Equation 3.5.[5]

$$\gamma_{obs} = \frac{A_h}{A_s}\left(\frac{I_o - I}{I}\right) \tag{3.5}$$

Equation 3.5 is used to determine the uptake of ethanol on the SiO_2 surfaces. In Equation 3.5, I_o is the mass spectrometer signal in the absence the reactive surface. In order to determine I_o, the steady state signal is averaged before the sample is exposed. After determining I_o, the signal for each scan (I) is entered into Equation 3.5. The area of the aperture (A_h) is 0.0707 cm^2, and the area of the surface (A_s) is 3.243 cm^2. The result is shown in Figure 3.4, a plot of the observed uptake coefficient (γ_{obs}) against time.

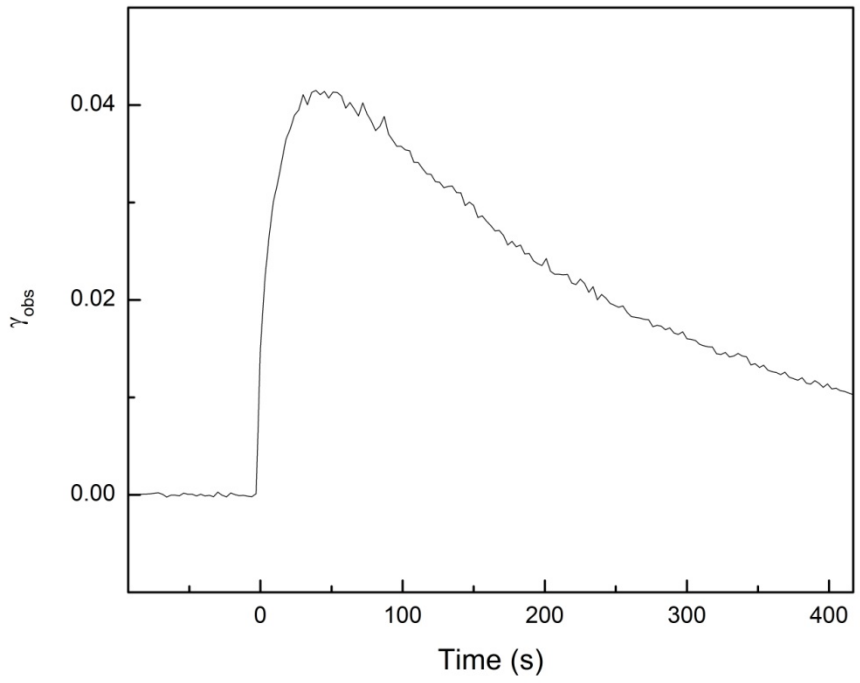

Figure 3.4 – Observed uptake vs. time for 99.1 mg of silica gel. The highest uptake point is used for each mass to calculate the average observed uptake. Surface was exposed at time 0 s.

Using the equations discussed above, the uptake coefficients for methanol and ethanol on SiO_2 and ethanol on activated charcoal were determined.

3.3.3. Knudsen Cell Performance Evaluation

3.3.3.1. Uptake of Ethanol on a Clean Sample Disc

Without a reactive surface present, the observed uptake of ethanol on a clean sample disc is expected to be zero. Figure 3.5 shows the observed uptake coefficient versus time for the clean sample disc.

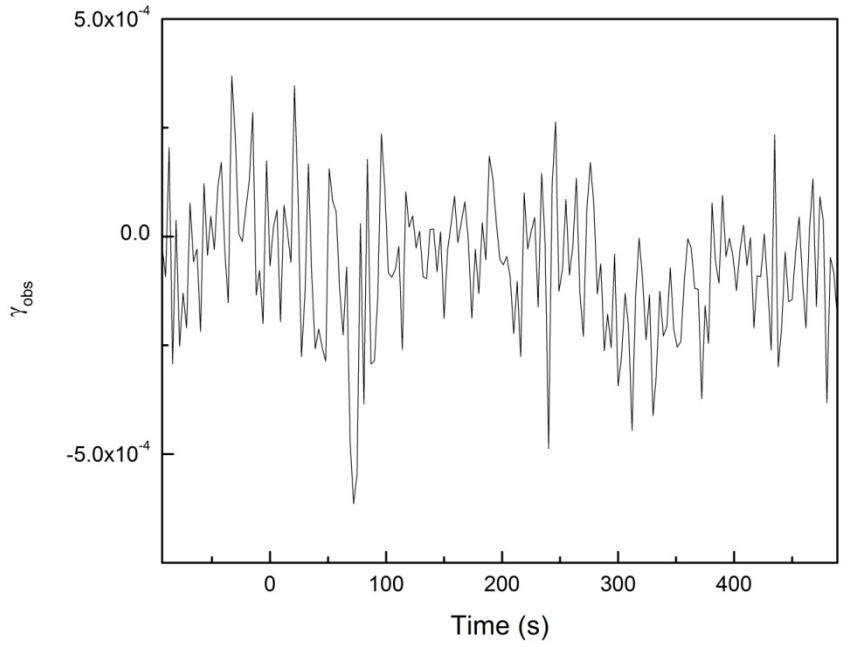

Figure 3.5 – Observed uptake versus time for one of the experiments performed on a clean, empty sample disc in the Knudsen cell. The sample was exposed at 0 s.

The uptake for the clean sample disc was calculated to be $(8 \pm 7) \times 10^{-5}$ (one standard deviation, n = 5). No discernible change was observed when the sample was exposed as seen in Figure 3.5. As the sample was exposed, at 0 s., no change in uptake occurred by simply raising the cap. Not only is no uptake observed for the clean sample disc, but this test shows that raising and lowering the cap over the surface has a negligible impact on observed uptake. The Knudsen cell performed successively in the first performance evaluation test because no uptake was observed for a clean sample disc.

3.3.3.2. Uptake of Methanol on Silicon Dioxide

The true uptake, which takes into account diffusion of the gas into the sample, of methanol on SiO_2 was used as a direct comparison to research previously completed by Carlos-Cuellar et al.[5] The true uptake coefficient measured in our cell is expected to be less than three orders of magnitude different from the coefficient calculated by Carlos-Cuellar et al.[5] A small

sample, 16.0 mg, of SiO_2 was exposed to methanol. The 16.0 mg sample was used in order to make the correction from observed uptake (γ_{obs}) to true uptake (γ_t) easier. For sample masses that fall within in the linear mass dependent regime a simple correction factor can be used to convert observed uptake to true uptake. (Equation 3.6)

$$\gamma_t = \frac{A_s}{A_{BET}}\gamma_{obs} \tag{3.6}$$

Equation 3.6 was used because based on the work done on this instrument and the work of Carlo-Cuellar et al. it was assumed that methanol could diffuse through the entire 16.0 mg sample. A_{BET} is the surface area in cm^2 of the sample. The surface area of the SiO_2 used in these studies was 500 m^2/g. The surface area was converted to 5000 cm^2/mg and multiplied by the sample weight, 16 mg, to obtain a A_{BET} of 80,000 cm^2. The true uptake coefficient for methanol on SiO_2 was determined to be $(5.6 \pm 0.3) \times 10^{-7}$. This value was only one order of magnitude different from the true uptake coefficient, $(4 \pm 2) \times 10^{-6}$, measured by Carlos-Cuellar et al.[5] Uptake coefficients measured for the same systems can vary between different research groups by one to three orders of magnitude.[5,59,60] Though the value was still an order of magnitude different from Carlos-Cuellar et al. uptake coefficients, possible reasons for this difference could be different sample conditions. The SiO_2 powder used in these studies has a different surface area compared to the powder used by Carlos-Cuellar et al.[5] Another thing to note from this study was the negligible effect pressure had on the true uptake coefficients. The true uptake of methanol on this SiO_2 was measured at two different exposure pressures in the uptake chamber.(Table 3.1)

Table 3.1 – True uptake coefficients determined for methanol on SiO_2 at two different pressures. Values are the average of three trials with a single standard deviation. The pressure difference had a negligible impact on uptake.

Uptake Chamber Pressure (Torr)	γ_t
1.7×10^{-4}	$(5.2 \pm 0.2) \times 10^{-7}$
2×10^{-6}	$(5.6 \pm 0.3) \times 10^{-7}$

The negligible impact on pressure showed the pumping differential setup in our chamber is adequate to eliminate any pressure dependence effects in the uptake measurements. A future quantitative study will use a similar silica sample to Carlos-Cuellar et al.[5] in order to obtain a more comparable true uptake coefficient. Thorough sample characterization, which our lab is adequately equipped to complete, will be paramount to ensure the use of similar samples to Carlos-Cuellar et al. for future work.

3.3.3.3. Surface Area Analysis

The goal of the final evaluation was to measure observed uptake coefficients proportional to the surface area of two different activated charcoal samples. For this study, two types of activated charcoal were used. The first consisted of granules with a surface area for 600 – 800 m^2/g, and the second was a fine powder with a surface area of 1400 m^2/g. This analysis requires the only difference in samples to be the surface area so the sample mass, 74.6 mg, and the ethanol dosing pressure was kept constant. The points on the plot of observed uptake versus surface area were obtained by averaging the maximum observed uptake of three different trials. Since the first activated charcoal sample has a surface area between 600 – 800 m^2/g, a value of 700 m^2/g was used to plot the data point. Figure 3.6 shows the data for the surface area analysis.

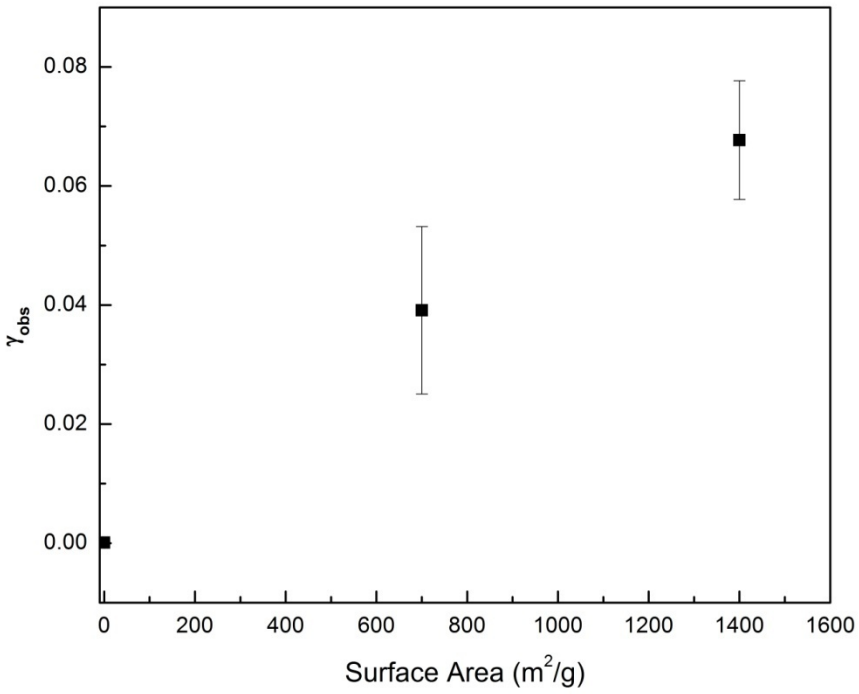

Figure 3.6 – Observed uptake plotted against the BET surface area of the activated charcoal samples. 95% confidence intervals are graphed for each point. The ratio between the two points is 1.73. The average uptake calculated for a clean sample disc was plotted.

The ratio between the two samples was 1.73. Based on the surface areas of the two types of charcoal, the ratio of the surface areas was between 2.33 and 1.75. The uptake ratio showed good agreement with the surface area ratio. The calculated ratio could be slightly less due to possible differences in the sample mass. Changes in sample mass could occur while preparing the sample or during the initial pump down. Another reason for the discrepancy could be the loosely packed granules for the charcoal sample with a surface area of 600-800 m^2/g. The loose packing of the granules could have resulted in more of the surface of the individual granules available to the ethanol to adsorb too. Despite the sources of error, the ratio of 1.73 proved the Knudsen cell can measure observed uptake proportional to surface area. The Knudsen cell

performed sufficiently on the three evaluations administered proving the instrument was ready to be used to study the uptake of ethanol on SiO_2.

3.3.4. Uptake of Ethanol on Silicon Dioxide

The linear mass dependent regime discussed in Chapter 1 was used to determine the true uptake of ethanol on SiO_2. To determine the true uptake of ethanol on SiO_2, the observed uptake was measured for different sample masses of SiO_2 including, 7.6, 13.5, 25.8, 55.2, and 99.1 mg. Figure 3.7 plots the observed uptake versus sample mass. A control point, 0 mg of SiO_2, was graphed in order to determine the true uptake of ethanol on the silica gel samples used. Each point on the plot is the average of the maximum observed uptake for five individual trials. The observed uptake increased linearly at first, after 25.8 mg, the observed uptake begins to level off.

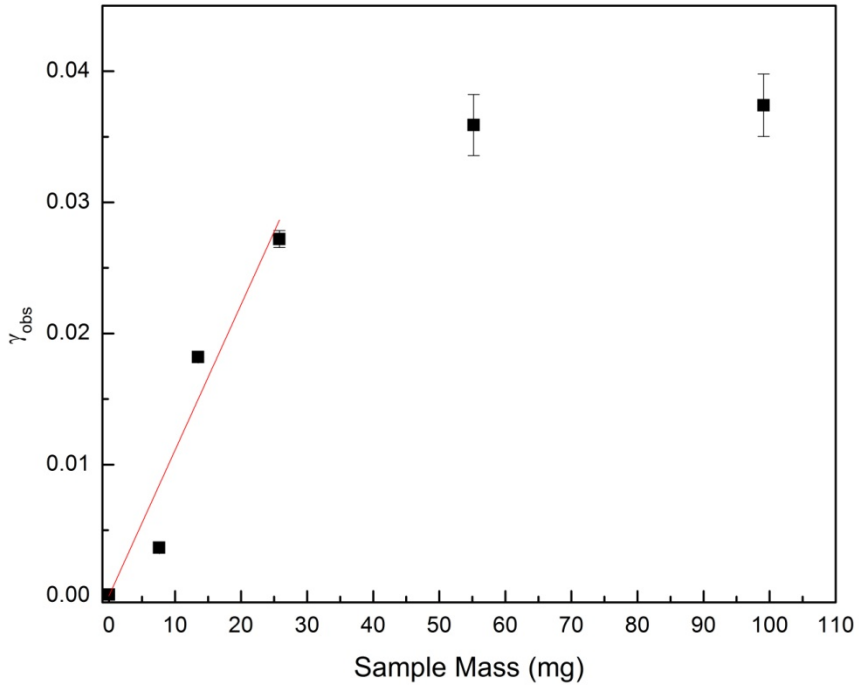

Figure 3.7 – Plot of observed uptake vs. sample mass. The linear increase can be followed from 0 – 25.8 mg. After which the observed uptake changes very little with sample mass. 95% confidence intervals are graphed for each point as well. A control point is graphed for 0 mg of silica gel. The line of best fit of the linear region has an equation of $y = 0.00108x$.

For the smaller masses, the ethanol was lost on the entire surface because the layers of particles are thin enough for complete diffusion of ethanol through the entire surface. Once the mass exceeded 25.8 mg the ethanol no longer diffuses through the entire surface thus limiting the ethanol to be lost to the upper layers of the sample. The trend observed in this study was consisted with previous research of the uptake of gas phase species by mineral dust aerosols.[5,24,25,28,30,33,40,50,61] The observance of this trend in our work further demonstrated the validity of the instrument, and the data was highly reproducible as evident by the small error bars.

Using the data graphed in Figure 3.7, the true uptake of ethanol on SiO_2 was determined using the linear mass dependent regime. To determine the true uptake of ethanol the focus was given to the data in the linear region of the plot in Figure 3.7. The line of best fit was plotted for the linear region. The line shown in Figure 3.7 has a slope of 0.00108 mg^{-1} and an R^2 value of 0.96. Using the slope of the line graphed in Figure 3.7, the true uptake coefficient was determined using Equation 3.7.[5]

$$\gamma_t = \text{slope } (\text{mg}^{-1}) \frac{A_S(\text{cm}^2)}{S_{BET}(\text{cm}^2\text{mg}^{-1})} \tag{3.7}$$

S_{BET} is the surface area of SiO_2 used in this study and is defined as 5000 cm^2/mg. The slope and A_s used in Equation 3.6 is 0.00108 mg^{-1} and 3.243 cm^2 respectively. The true uptake for ethanol on the SiO_2 powder used here is 7×10^{-7}. A comparison of the uptake coefficient of ethanol on SiO_2 to the uptake of gas phase species is shown in Table 3.2.

Table 3.2 - True uptake coefficients of various compounds measured on SiO_2. The uptake of ethanol calculated in this work is not the smallest, but there are other compounds that have a higher chance of being lost on the surface than ethanol.[5,26,28,37,46]

Uptake Coefficients of Various Compounds on Silicon Dioxide	
Compound	**γ_t**
Ozone	$(6.3 \pm 0.9) \times 10^{-5}$
Nitric Acid	$(2.9 \pm 0.2) \times 10^{-5}$
SO_2	$< 1 \times 10^{-7}$
Acetic Acid	$(2.4 \pm 0.4) \times 10^{-4}$
Methanol	$(4 \pm 2) \times 10^{-6}$
Formaldehyde	$(2.6 \pm 0.9) \times 10^{-7}$
Acetaldehyde	7.0×10^{-6}
Acetone	6.2×10^{-6}
Propionaldehyde	1.1×10^{-5}
Ethanol(this work)	7×10^{-7}

The loss of ethanol on SiO_2 in the atmosphere would be more likely than the loss of SO_2 and formaldehyde; however, there are several compounds that are far more likely to be lost on the surface of SiO_2 before ethanol. Ethanol lost to gas phase reactions with OH radicals is more likely than the loss of ethanol to SiO_2.[5] The true uptake coefficients calculated here was the

result of only one set experiments studying the uptake of ethanol on SiO_2, and to improve the accuracy of this value, more experiments studying the uptake of ethanol on SiO_2 are required.

3.3.5. Infrared Spectroscopy Data

Fourier transform infrared spectroscopy (FTIR) was used to determine how ethanol is lost to the SiO_2 surface. The data shown here was done in a ultra high vacuum (UHV) system equipped with a capillary array doser to expose silicon dioxide to ethanol. Absorbance IR spectra of the silica nanoparticles were gathered during the dosing. Nanoparticles with a surface area of 200 m^2/g were used. Despite the difference in surface area, the data gathered here can be applied to the SiO_2 used in the Knudsen because the samples were comprised of the same oxide. Figure 3.8 shows a difference IR spectrum after over ~90 minutes of dosing the surface with ethanol at a pressure of 10^{-6} Torr.

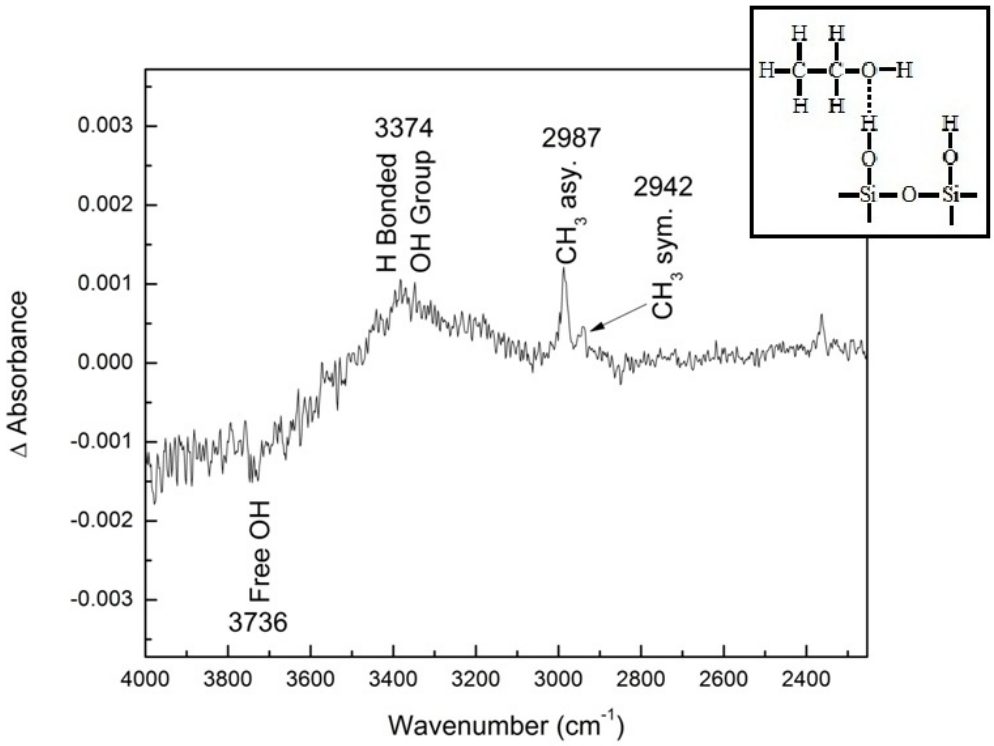

Figure 3.8 – Difference spectrum of SiO_2 nanoparticles after over 90 minutes of ethanol dosing. Spectrum is the result of 128 scans. The slight loss in free OH groups with the increase in hydrogen bonded OH demonstrates how ethanol is lost to the SiO_2.

The loss of free OH groups suggests the ethanol is hydrogen bonding to the terminal hydroxyl groups on the surface of SiO_2. The mechanism is depicted in the small image in the upper right corner of Figure 3.8.[41] The peak assignments were compared to the work of Natal-Santiago et al.[62] in Table 3.3.

Table 3.3 –Vibration modes observed between this work and Natal-Santiago et al. for the adsorption of ethanol on the surface of SiO_2 and the gas phase IR modes of ethanol.[62]

IR Peak Comparison of Ethanol on Silicon Dioxide			
Vibration Modes	**Natal-Santiago et al. (cm^{-1})**		**This work (cm^{-1})**
	Gas Phase	Surface Adsorbed	Surface Adsorbed
ν(OH)	3676	3740	3736
ν(OH)		3326	3374
$\nu_{as}(CH_3)$	2989	2982	2987
$\nu_{s}(CH_3)$	2943	2932	2942

The surface adsorbed vibration modes observed in our work were different from those observed by Natal-Santiago et al. The gas phase modes of ethanol are closer to the surface adsorbed modes observed in our research. Similarities between the surface adsorbed modes and the gas phase modes reported by Natal-Santiago et al. implies the ethanol weakly bonds to the surface of SiO_2.[5,62] The differences between the surface adsorbed modes observed in both studies could be caused by differences in sample prep prior to the experiments. Natal-Santiago et al. heated their samples to 600 K for two hours to remove any adsorbed compounds before dosing the surface with ethanol. In our study, the sample was not heated prior to exposure because the samples in the Knudsen cell were not heated prior to experiments. Without heating, the surface may have had some adsorbed contaminants on it that could interfere with adsorption of ethanol on the surface. The IR data suggests that hydrogen bonding between the terminal hydroxyl groups on the surface of SiO_2 is the pathway through which gas phase ethanol is lost on the surface.

3.4. Summary

The data collected in the above studies validated the performance of the Knudsen cell as an effective tool with which to measure the uptake of gas phase reactants on well characterized surfaces. The observed uptake versus sample mass was consistent with published work involving uptake of chemical compounds on mineral dust aerosols. The Knudsen cell performed adequately on the benchmark evaluation studies conducted in the cell. No uptake was observed for the blank, no SiO_2 present, sample. A comparable true uptake coefficient to previously published work for methanol on SiO_2 was obtained in our cell. Finally, obtaining observed uptake coefficients comparable to the surface area of two different charcoal samples demonstrated the Knudsen cell was operating efficiently to begin studies on systems not previously studied. The true uptake of ethanol was found to be competitive with only a few other

atmospheric compounds, but overall, the loss of ethanol on mineral dust aerosols would not be competitive with other prevalent atmospheric species such as nitric acid. These studies have thoroughly tested the Knudsen cell. With the Knudsen cell successfully performing within these experiments, it is ready to be used in other projects currently in progress in this research lab.

3.5. Future Work

The Knudsen cell will be used in the future to expand our knowledge of heterogeneous systems already being studied by our lab. Our lab currently studies the adsorption of chemical warfare agent simulants (CWAs) and in the future the uptake of these simulants on surfaces will be studied in the Knudsen cell. A great deal of atmospheric chemistry involving ozone reactions with organic surfaces have been studied in this lab. Ozone uptake on C_{60} molecules and the uptake of NO_3 radicals on various surfaces will be studied with the Knudsen cell in the future. The proposed work will help expand the understanding of important heterogeneous chemical pathways in the atmosphere.

Chapter 4

Development of a Nitrate Radical Source

4.1. Introduction

The Knudsen cell described in Chapter 2 will be used in future work to study the uptake of nitrate radicals (NO_3) on atmospherically relevant surfaces. Modeling studies done by Dentener et al[34,35] proposed that under dry conditions the uptake of NO_3 and dinitrogen pentoxide (N_2O_5) on mineral dust aerosols would be negligible. Adsorbed moisture on the surface has the potential to enhance the uptake of NO_3 on mineral dust aerosols. The mechanism for the loss of NO_3 on mineral dust aerosols is not well understood and there are few literatures sources on this reaction.[34,35] The goal of future work is to study the reactive uptake of NO_3 on mineral dust aerosols.

4.2. Nitrate Radicals

NO_3 was first identified by two French scientists using spectroscopic methods.[63,64] In 1881, Hautefeuille and Chappuis observed the absorption bands of pure ozone (O_3) over time and a mixture of O_3 and nitrogen that had an electric current passed through it. The researchers noted the presence of absorption bands of O_3, but at the same time a series of unique absorption bands were observed at 662 and 623 nm, indicating the presence of NO_3.[63,64] There is a need to understand the role of this chemical species in the atmosphere.

In the atmosphere, the behavior of NO_3 is dictated by the temperature, amount of sunlight, and the presence of certain gas molecules that can react with NO_3.[65-71] NO_3 is produced in the atmosphere via the oxidation of NO_2 and O_3 (Reaction 4-A).[64-66,69]

$$NO_2 + O_3 \rightarrow NO_3 + O_2 \qquad (4\text{-A})$$

Once formed, NO_3 decomposes in sunlight to form either nitrogen monoxide (NO) or NO_2. If the photolysis of NO_3 produces nitrogen monoxide and diatomic oxygen, a net reaction occurs resulting in the breakdown of O_3.(Reactions 4.B – 4.E) If NO_2 and oxygen are the products of the photolysis reaction, there is no net effect on O_3.[65]

	$NO_3 + h\nu \rightarrow NO + O_2$	(4-B)
	$NO + O_3 \rightarrow NO_2 + O_2$	(4-C)
	$NO_2 + O_3 \rightarrow NO_3 + O_2$	(4-D)
Net	$2\ O_3 + h\nu \rightarrow 3\ O_2$	(4-E)

NO_3 not only impacts ozone levels in the atmosphere, but also interacts with aerosol particulate matter in the atmosphere.[1] Compounds that NO_3 can react with include aqueous solutions[72,73], salt aerosols[74,75], polycyclic aromatic hydrocarbons[76,77], and saturated/unsaturated organic compounds.[78,79] The uncertainty behind the mechanisms of the reactions between NO_3 and the compounds listed above requires more research to gain a better understanding of atmospheric chemistry. In an effort to improve the understanding of NO_3 chemistry in the atmosphere, work was done to develop a NO_3 gas source for use with existing vacuum chambers in the laboratory.

One of the most common methods for production of NO_3 was first proposed by Schott and Davidson in the 1950s.[80] While researching the kinetics of N_2O_5, Schott and Davidson provided the scientific community with an easy, effective method to produce NO_3. The process (Figure 4.1) started with the purification of O_2 by passing it through a section of tubing kept at -80^{o}C.

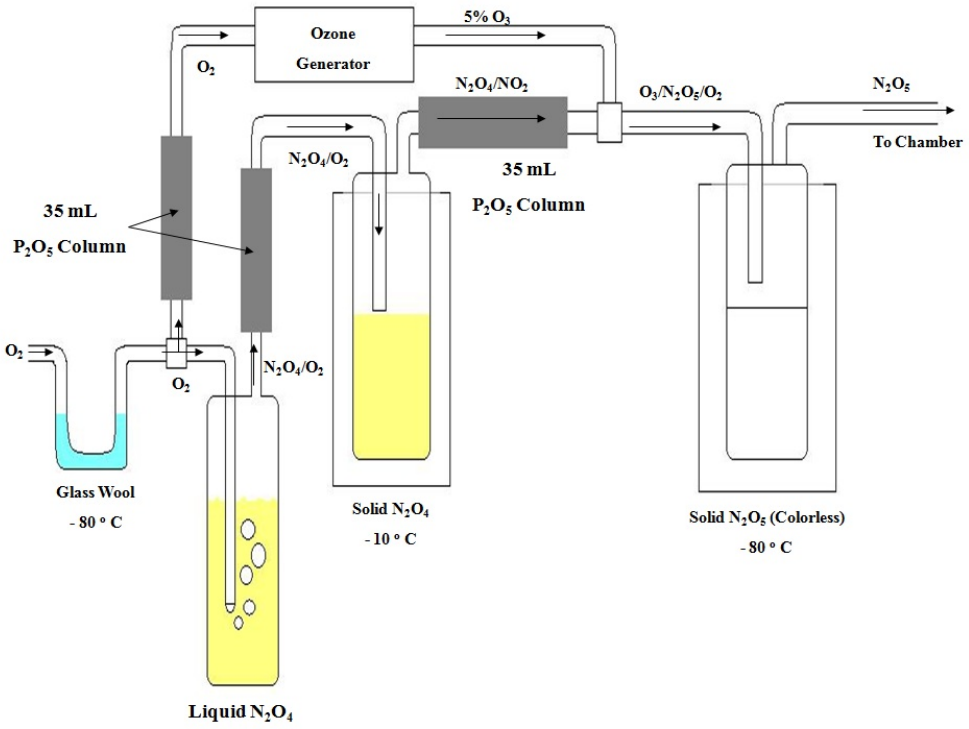

Figure 4.1 –A schematic diagram of Schott and Davidson's production method as described in their paper.[80]

The oxygen stream was divided into two directions. One path took the oxygen through a column packed with glass beads coated in phosphorous pentoxide (P_2O_5) on its way to an ozone generator, and the other path flowed through a glass trap filled with liquid N_2O_4. The O_2-N_2O_4 gas stream passed through another P_2O_5 column into a collection trap maintained at -10°C. The N_2O_4 trap was warmed slightly to release a stream of NO_2-N_2O_4, which passed through a P_2O_5 column, and reacted with a 5% O_3 stream from the ozone generator. The resultant stream, O_2-N_2O_5-O_3, passed through a foot of tubing. The foot of tubing was used to visually inspect the gas to ensure it is colorless. Lack of color in the tube indicated only N_2O_5, O_3, and O_2 were present. The N_2O_5 crystals were collected in a second collection vessel cooled to -80°C. NO_3 radicals were produced by dissociating the N_2O_5 gas by heating it between 450 – 600 K.(Reaction 4-F)

$$N_2O_5 \rightarrow NO_2 + NO_3 \qquad (4\text{-F})$$

The equilibrium constant for Reaction 4-F is 5×10^{-5} moles per liter at 450 K and increases with increasing temperature.[80] The system used by Schott and Davidson is the foundation for our attempts to make NO_3 radicals. The development of the system went through several stages.

4.3. Experimental Setup

The development of this NO_3 source went through many different stages of trial and error. Since the production of NO_3 involves the use of highly toxic and corrosive gases (i.e. NO_2 and NO), the system was designed to fit into a fume hood to protect researchers in the laboratory. The first version of the NO_3 source is shown in Figure 4.2.

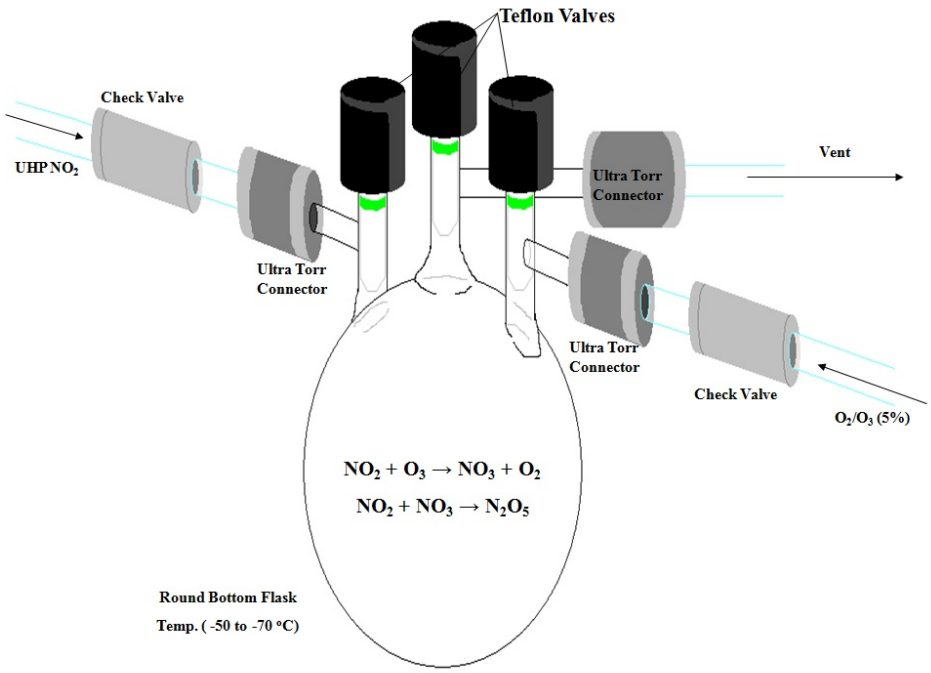

Figure 4.2 – First version of the NO_3 production source designed for this research. It consisted of a single round bottom flask.

The first version of the N_2O_5 source consisted of a custom 500 mL round bottom flask with three necks, each containing a Teflon® valve. Connections between the glass flask and the Teflon tubing (McMaster-Carr®, RS-85017080) were made with Ultra-Torr® vacuum fittings (Swagelok®, SS-4-UT-6). Check valves (Swagelok®, SS-4C-1/3) were placed on the gas lines

for NO_2 and $O_2/O_3/N_2$ in order to direct the gas flow in one direction and prevent any mixing of the reactant gases in the Teflon® lines. The first setup reduced the three trapping vessels in Schott and Davidson's method to a single trapping vessel for both producing and trapping the N_2O_5.

Trapping N_2O_5 in the first setup was done as follows. The Teflon® valve on the vent line was opened during the N_2O_5 trap to avoid pressure build up in the round bottom flask. Ultra high purity (UHP) nitrogen (N_2) was introduced to the system through the O_2/O_3 line to purge the system for three minutes. After 3 minutes, UHP O_2 purged the system for another five minutes. Once five minutes had elapsed, a commercially available ozone generator (not shown above) was turned on to purge the system with ozone for five to ten minutes. O_3 purged the walls of the system of any adsorbed hydrocarbon contaminants. UHP NO_2 (Matheson Tri-Gas®, G1558169) was introduced into the round bottom flask by opening the left most Teflon® valve in Figure 4.2. As soon as the gases began mixing, the round bottom flask was lowered into an ethanol/dry ice bath which cooled the flask to between -50 and -70^oC. White powder (Figure 4.3) formed on the bottom of the flask shortly after it was lowered into the ice bath. NO_2 and O_3 were allowed to mix in the round bottom flask for one hour.

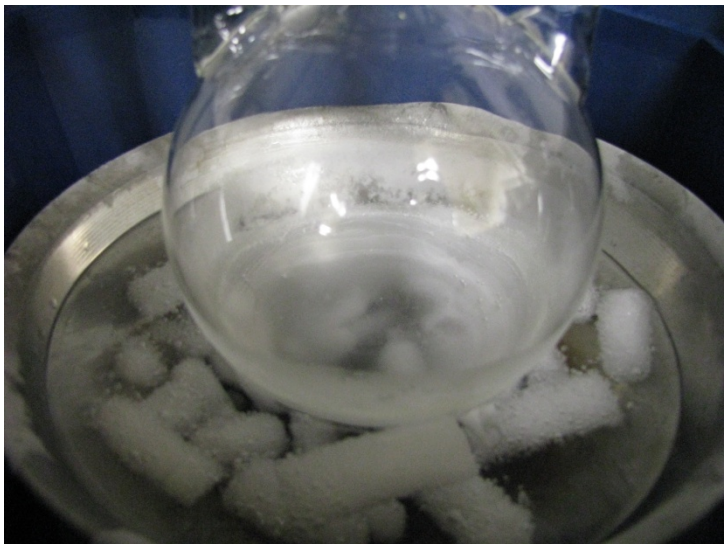

Figure 4.3 – White powder, supposedly N_2O_5, collected in the round bottom flask after one hour of trapping.

After one hour, the left Teflon® valve was closed and the ozone generator turned off. UHP N_2 purged the system for ten minutes. The flask was raised out of the bath after the N_2 purge and the color of the gas from the sublimating crystals was examined. It was determined by the presence of brown gas, the white powder collected in the round bottom flask was contaminated with NO_2. Attempts to characterize the gas with UV-Vis spectroscopy yielded no definitive proof of N_2O_5. The absence of N_2O_5 in the UV-Vis spectrum was due to the small amount of white powder trapped after an hour or more of trapping. Leaving the vent line opened was determined to be the reason for the small yield of white powder, because any N_2O_5 produced would be lost through the vent line before being trapped.

To fix this problem, the system was modified to contain two glass chambers, one for mixing the reactants and one for trapping the product. The new system (Figure 4.4) was designed to be fully contained from the atmosphere.

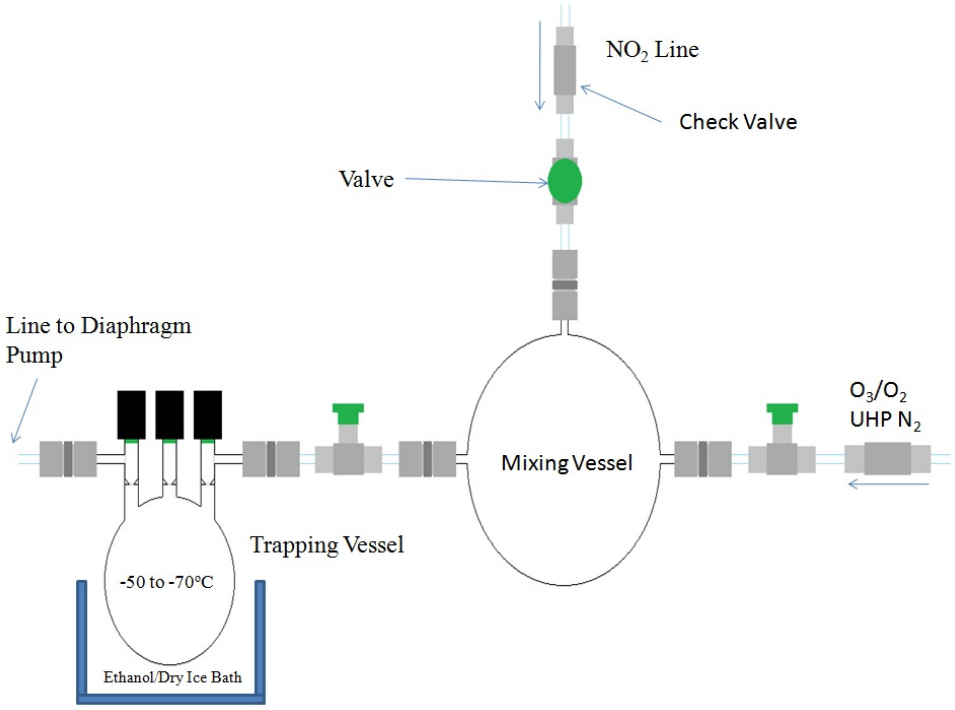

Figure 4.4 – Schematic of the second version of the NO_3 source.

Once isolated from the atmosphere, with all valves in Figure 4.4 open, the system was evacuated by a diaphragm pump (not shown) for twenty minutes. The valves were then closed and the round bottom flask was cooled with an ethanol/dry ice bath. The mixing vessel was filled with NO_2 until a faint brown color was apparent and the valve on the NO_2 line was closed. The O_3 generator was turned on and O_3 was allowed to fill the Teflon® tubing up to the O_3/O_2 valve. Upon opening the O_3 valve, the brown color in the mixing vessel disappeared and the ozone flow was stopped. The pressure differential between the mixing vessel and the trapping vessel, which had been isolated from the mixing vessel, was used to draw any N_2O_5 in the mixing vessel into the cooled trapping vessel. When the valve between the two vessels was opened, no white powder appeared. In an effort to draw more of the product gas from the mixing vessel into the trapping vessel, the system was pumped on by the diaphragm pump with the trapping vessel cooled to keep any product gas from being pumped out of the system. This yielded no white powder even after pumping on the system for thirty minutes. When the pressure in the system

was brought up to atmospheric pressure, a white film appeared on the mixing and trapping vessels. The white film was believed to be N_2O_5 or HNO_3, a product of a N_2O_5 hydrolysis.[81] The second version of the system yielded less white powder than its predecessor. Separating the mixing and trapping vessels, similar to Schott and Davidson's method, was believed to not be the cause of the problem.

The possible reason behind the absence of any trapped N_2O_5 was the pressure at which the trapping occurred. Without a pressure gauge on the system there was no way to know at what pressure the trapping occurred. The pressure could have been too low to condense the N_2O_5. The vapor pressure of N_2O_5 (Table 4.1) confirmed our theory of the pressure being too low to condense the N_2O_5 at the temperatures of the ethanol/dry-ice bath.[82]

Table 4.1. – A compiled table showing the physical phase of N_2O_5 at various pressures. N_2O_5 sublimes just above freezing at atmospheric pressure.[82] Physical state of N_2O_5 is denoted next to each temperature: S for solid and G for gas.

Physical Phase of N_2O_5 at Various Pressures						
Pressure	1 Pa	10 Pa	100 Pa	1 kPa	10 kPa	100 kPa
Temp (^oC)	- 71 [S]	-56 [S]	- 40 [S]	- 19.9 [S]	3.9 [S]	33.2 [G]

The ethanol dry ice bath maintained the trapping flask at a temperature of -50 to -70^oC . From Table 4.1, if the pressure was above one Pascal, N_2O_5 would have solidified. At atmospheric pressure, the table shows that N_2O_5 sublimes just above room temperature. If the trapping were to occur at atmospheric pressure the ethanol/dry-ice bath is expected to be sufficient to condense the N_2O_5.

The third version of the NO_3 source was designed as a flow system with the trapping of N_2O_5 occurring at atmospheric pressure. Nitrogen monoxide (NO) replaced NO_2 in this version to obtain a better flow of the gas into the mixing vessel.[74,83] A directional flow of reactant gases ensured the N_2O_5 reached the cooled trapping vessel. From these modifications, the third version

(Figure 4.5) of the NO_3 source was made with custom glassware to improve the chances of condensing N_2O_5 in the trapping vessel.

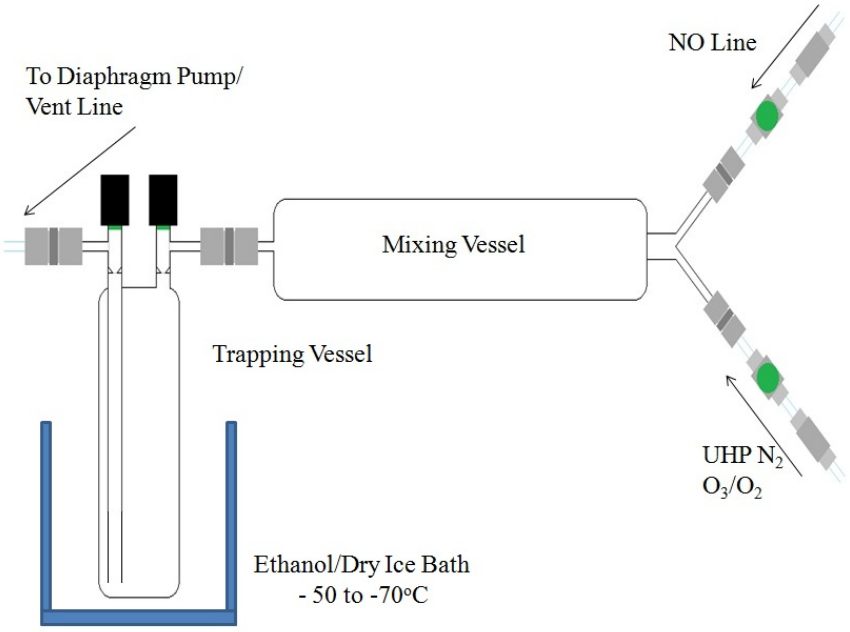

Figure 4.5 – The final version of the setup. It consists of custom glassware to ensure adequate flow of gases from the mixing vessel to the trapping vessel.

The mixing vessel is a glass tube, ~16 in. in length and ~ 2.75 in. in diameter. The ends are reduced to quarter inch glass tubing connections. On one end of the mixing vessel, the quarter-inch glass connections intersect to ensure the reactant gases mix and react before flowing down the length of the vessel. The glass trapping vessel is ~ 8 in. in height and ~ 2 in. in diameter. It is contained by two Teflon® valves. A glass tube extends from the vent line of the setup to just above the base of the trapping vessel, forcing the gases to travel to the base of the trapping vessel. Once the gas reaches the base of the trapping vessel, N_2O_5 condenses out of the gas phase, and the O_3/O_2 would flow out of the system. Connections on the setup were made with Ultra-Torr® vacuum fittings, and bellows sealed valves (Swagelok®, SS-4H) contained the reactant gases. The third version of the setup was expected to be the most successful based on the changes made on the setup for synthesizing N_2O_5.

4.3.1. N_2O_5 Trapping Procedure

N_2O_5 was trapped in the third setup following the procedure detailed below. The system was evacuated with a diaphragm pump back to the O_3 generator and the NO regulator for thirty minutes. After thirty minutes, the valves to the NO tank and the diaphragm pump were closed. The system was disconnected from the diaphragm pump, and the line with which the pump was connected was placed up in the hood to act as a vent line during the trapping process. UHP N_2 filled the system, which was opened to the vent line to avoid overpressurization. After a five minute N_2 purge, UHP O_2, ~ 5 psi, purged the system for an additional five minutes. The system was purged with O_3 for ten minutes before NO is introduced. Only a small amount of NO was required and the regulator was only cracked open to allow for a small stream of NO to enter the system. When the NO intersects the O_3/O_2 stream, the gas was oxidized to form NO_2 confirmed by the presence of brown gas. (Figure 4.6)

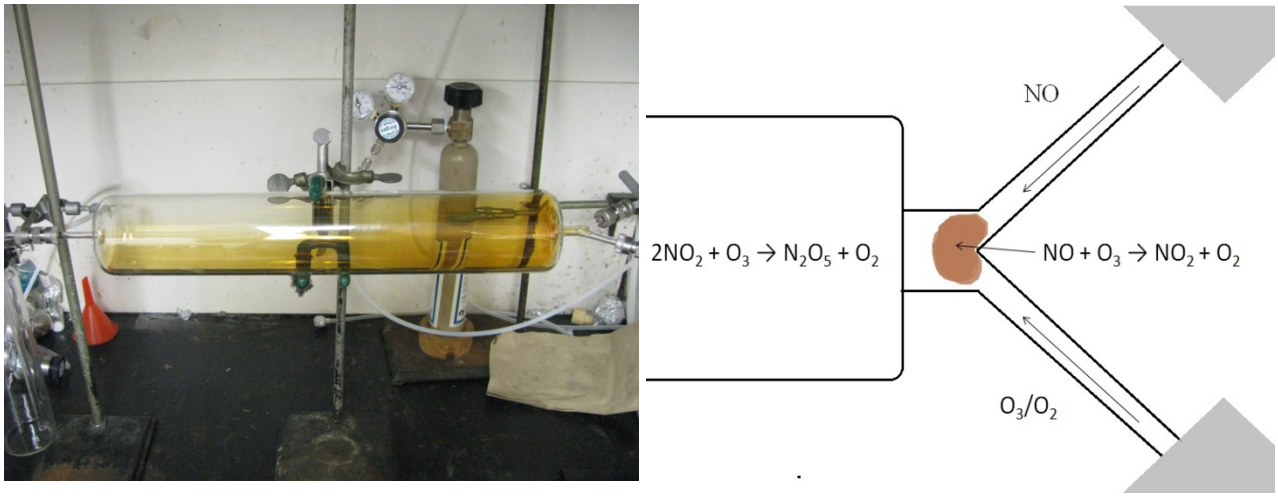

Figure 4.6 – Left panel shows the oxidation of NO to NO_2, brown gas present in the mixing vessel. Right panel drawing of the ideal flow state of NO and O_3/O_2.

The NO flow was reduced until the ideal flow state, shown in the right diagram of Figure 4.6, was achieved. The NO_2 produced by the initial oxidation was oxidized again to N_2O_5. Once the ideal flow was achieved, the trapping vessel was cooled with an ethanol/dry ice bath. Upon

cooling the trapping vessel, white crystals began to grow on the sides of the vessel. Trapping was allowed to proceed for three to four hours. Next, the system was purged with UHP N_2 to clear out any residual $N_2O_5/NO_2/O_2/O_3$ from the system. The collected crystals were kept cool until they were characterized using UV-Vis and IR spectroscopy.

Figure 4.7 – N_2O_5 crystals collecting at the base of the trapping vessel.

4.3.2. Characterization of N_2O_5

UV-Vis and IR spectroscopy were used to determine the chemical compound of the white crystals collected. Talawar et al.[84] stated that N_2O_5 has characteristic absorption peaks at 200 and 380 nm. NO_3 radicals absorb light at 623 and 662 nm.[63] The trapping vessel was connected to a different flow system (Figure 4.8) equipped to heat the sublimed gas to 450 – 600 K. In order to heat the gas to these temperatures, the system was equipped with a six inch glass tube wrapped in nichrome wire. The nichrome wire was heated by flowing a current through it. The gas flowed through the heating tube into a quartz cuvette placed between two fiber optic cables, one for the UV light source and one connected to the detector.

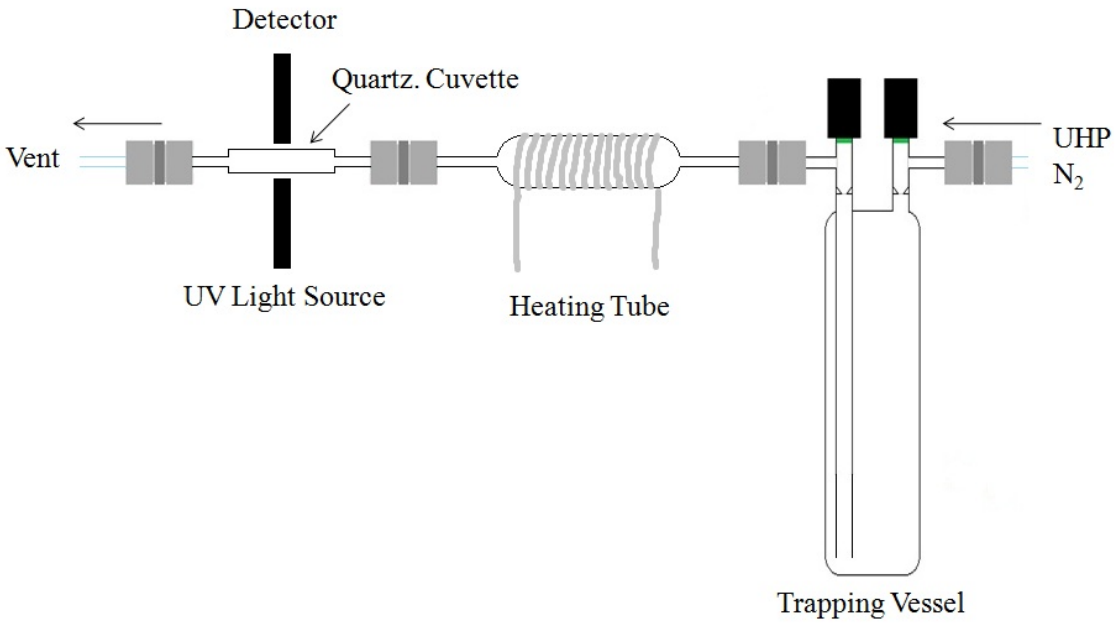

Figure 4.8 – Schematic of the UV-Vis spectroscopy set up used to characterize N_2O_5 and NO_3. UHP N_2 was used a carrier gas.

The UV-Vis spectrum (not shown) failed to provide conclusive results to the presence of NO_3 in the gas stream after it was heated. Broad peaks around 200 and 380 nm, which suggests N_2O_5 was present, appeared as the trapping vessel warmed and the temperature of the heating wire increased. Despite the fact that the heating tube had reached the temperatures printed in literature to dissociate the N_2O_5 into NO_3 radicals, there were no peaks in the UV-Vis spectrum at 662 and 623 nm.

Gas phase IR spectroscopy was used to provide further evidence that N_2O_5 was produced using the trapping method described for the third version of the NO_3 source. The trapping vessel was placed in line with a flow cell (Figure 4.9) that was originally designed to study the reactions of chemical warfare simulants on metal oxides. The N_2O_5 crystals were gradually warmed to room temperature, and the N_2O_5 gas was carried to the flow cell with UHP He.

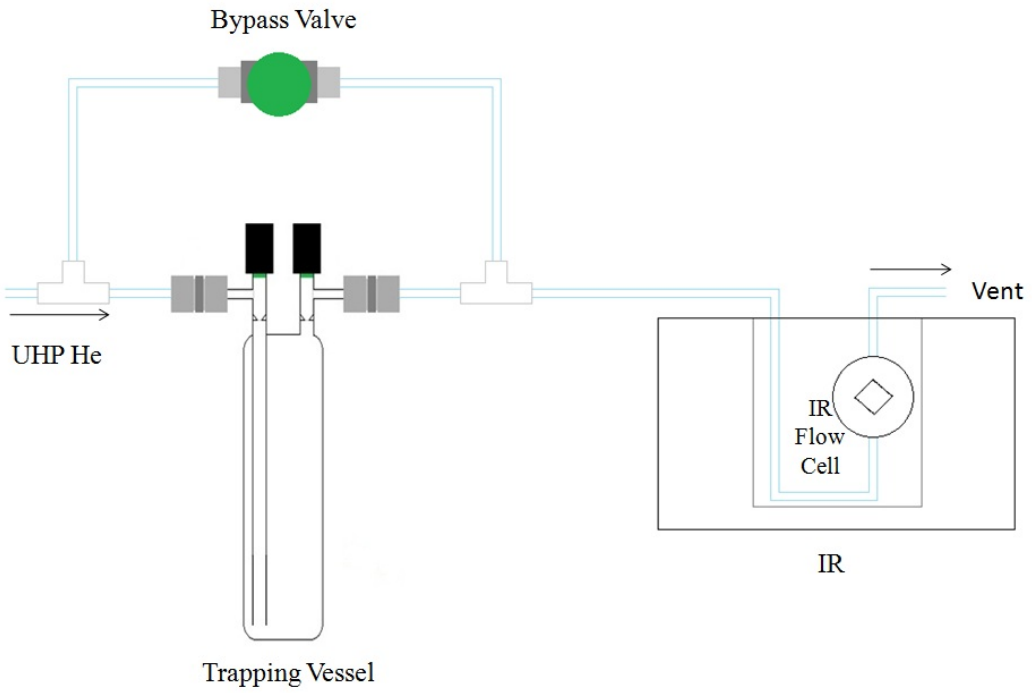

Figure 4.9 – Schematic of the N_2O_5 setup in line with the IR flow cell for the purpose of obtaining gas phase IR spectrum.

IR spectra were collected with a Nexus 470 FTIR spectrometer equipped with a liquid nitrogen cooled MCT (Mercury Cadmium Telluride) detector with a range of 700 to 4000 cm^{-1}. A background spectrum was collected by flowing UHP He through the bypass with the trapping vessel closed. After collecting the background spectrum, the bypass valve was closed, and the trapping vessel opened to the flow cell. UHP He carried the gas from the trapping vessel into the IR flow cell. IR spectra were scanned against the background collected to identify the chemical species in the trapping vessel.

4.4. Results and Discussion

The trapped white crystals were warmed, and the sublimed gas flowed into the IR flow cell where the data collected indicated the presence of N_2O_5. As the crystals warmed up, IR peaks were observed between 700 and 2400 cm^{-1}. The intensity of the peaks increased as time went on.

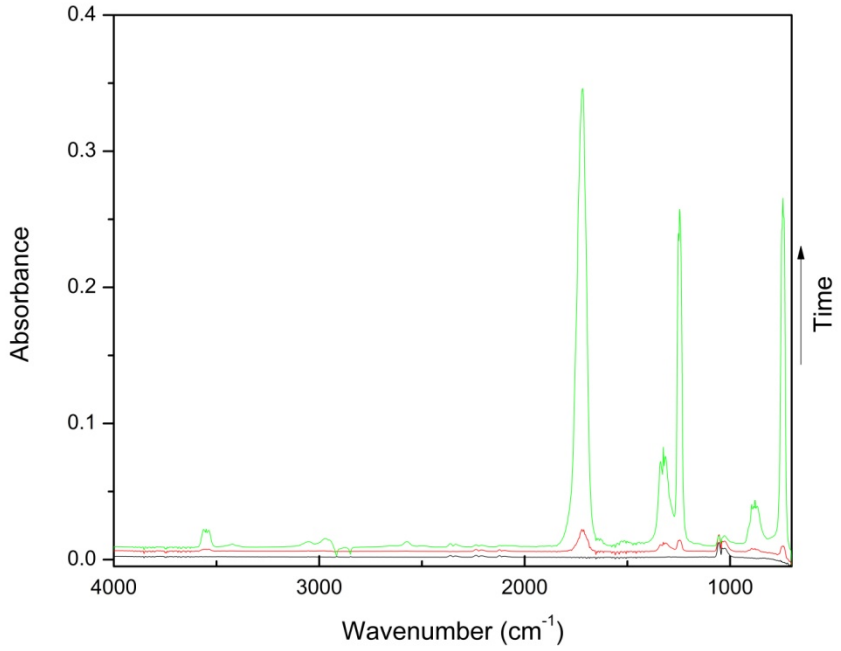

Figure 4.10 – IR spectra collected over time of gas phase species from the warmed trapping vessel.

The largest peaks were observed at 1715 cm^{-1}, 1329 cm^{-1}, 1244 cm^{-1}, 877 cm^{-1}, and 740 cm^{-1}. These peaks were only present in the first fifteen minutes of warming the N_2O_5. After fifteen minutes, the peaks became obscured as the gas reacts with adsorbed hydrocarbons, indicated by negative peaks around 2800 cm^{-1}, and water in the flow cell. The analysis focused on the five most intense peaks in the above spectra. (Figure 4.11) The peaks observed here were compared to work done by Wassell et al.[85] Wassell et al. reacted NO_2 and O_3 to produce N_2O_5 in a gas flow system. Their IR spectrum is consistent with the spectra collected in this work.

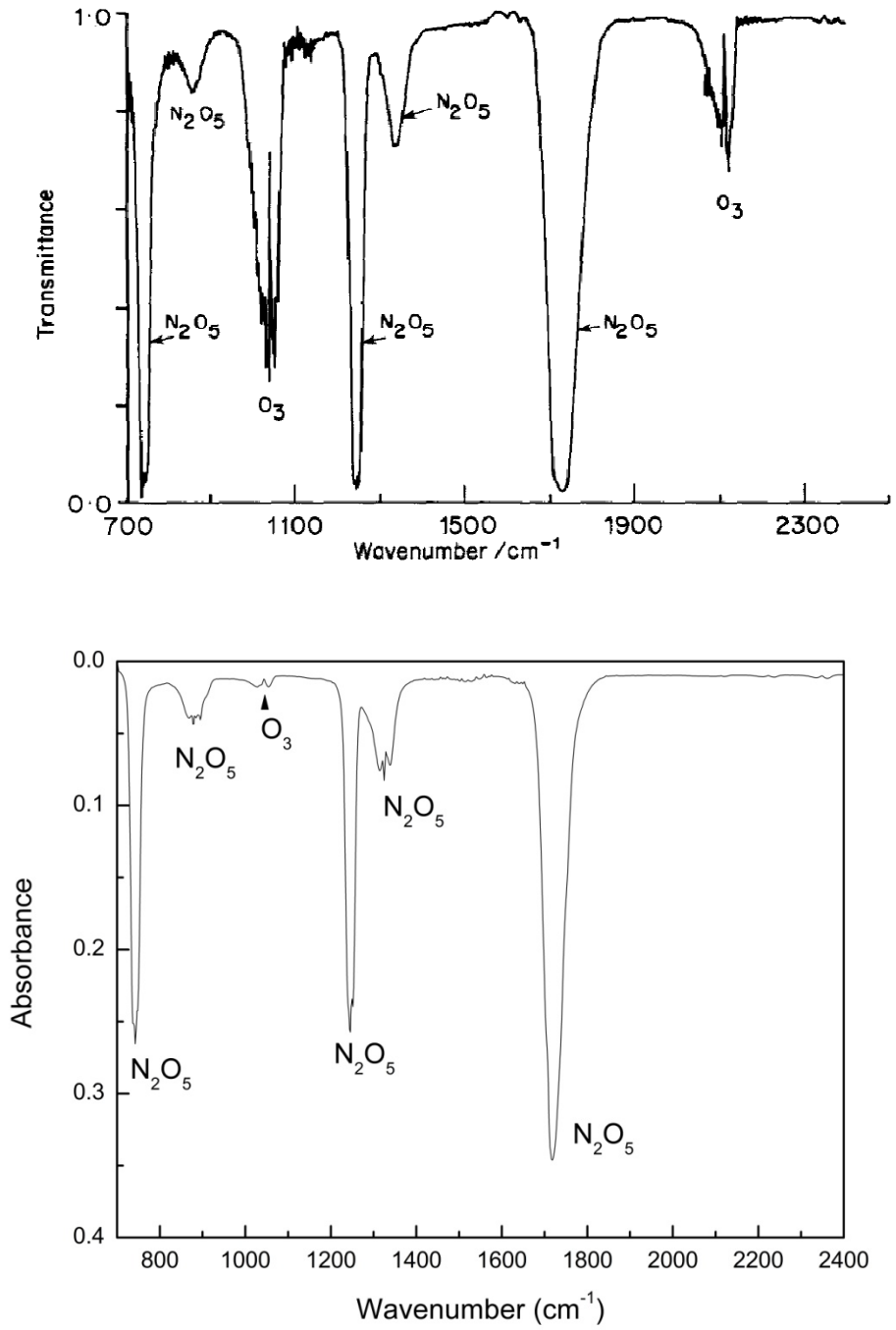

Figure 4.11 – (Top) FTIR spectrum of N_2O_5 collected by Wassell et al.[85] Reprinted with kind permission from Springer Science+Business Media: Journal of Atmospheric Chemistry, Laboratory Spectroscopic Studies of Atmospherically Important Radicals Using Fourier Infrared Spectroscopy, 8, 1989, pg 69, Wassell et al.[85], Figure 2, Copyright 1989. (Bottom) FTIR spectrum of N_2O_5 collected from this research. Spectrum was flipped upside down to make the visual comparison easier.

The spectrum obtained in our research showed good agreement with the spectrum published by Wassell et al. After the first fifteen minutes, the observed peaks became obscured with other product peaks. These peaks were likely the result of reactions that occur in the gas phase and on the walls of the cell. Though UV-Vis spectroscopy yielded no definitive proof of NO_3, the IR spectra collected in this study confirmed the successful synthesis of N_2O_5.

4.5. Conclusion and Future Outlook

The IR and UV-Vis spectra collected in this study suggest that N_2O_5 was synthesized with the developed setup. No evidence of NO_3 radicals was observed even when heating the gaseous N_2O_5. It is possible the small yield of N_2O_5 was not enough to produce a detectable amount of NO_3. The method for heating the gaseous N_2O_5 may not have been adequate to efficiently break it down. Future work on the system will include using a new ozone generator with a higher ozone output and modifying the way the N_2O_5 is thermally broken down. Once a stable, reproducible NO_3 source is developed, it will be utilized to study the reactive uptake of NO_3 on different surfaces in the Knudsen cell.

Appendix

Appendix A – Rights and Permissions

AMERICAN CHEMICAL SOCIETY LICENSE TERMS AND CONDITIONS

Apr 30, 2011

This is a License Agreement between Thomas H Rockhold ("You") and American Chemical Society ("American Chemical Society") provided by Copyright Clearance Center ("CCC"). The license consists of your order details, the terms and conditions provided by American Chemical Society, and the payment terms and conditions.

All payments must be made in full to CCC. For payment instructions, please see information listed at the bottom of this form.

License Number	2658400272832
License Date	Apr 29, 2011
Licensed content publisher	American Chemical Society
Licensed content publication	The Journal of Physical Chemistry A
Licensed content title	Heterogeneous Uptake Kinetics of Volatile Organic Compounds on Oxide Surfaces Using a Knudsen Cell Reactor: Adsorption of Acetic Acid, Formaldehyde, and Methanol on α-Fe2O3, α-Al2O3, and SiO2
Licensed content author	S. Carlos-Cuellar et al.
Licensed content date	May 1, 2003
Volume number	107
Issue number	21
Type of Use	Thesis/Dissertation
Requestor type	Not specified
Format	Print and Electronic
Portion	Table/Figure/Micrograph
Number of Table/Figure /Micrographs	1
Author of this ACS article	No
Order reference number	

Title of the thesis / Dissertation
Development of a Knudsen Cell Reactor for Measuring the Uptake of Atmospheric Gases on Particulate Matter

Expected completion date	May 2011
Estimated size(pages)	95

Billing Type	Invoice
Billing Address	880 Plantation Road Apartment 407 Blacksburg, VA 24060 United States
Customer reference info	
Total	0.00 USD
Terms and Conditions	

SPRINGER LICENSE TERMS AND CONDITIONS

Apr 30, 2011

This is a License Agreement between Thomas H Rockhold ("You") and Springer ("Springer") provided by Copyright Clearance Center ("CCC"). The license consists of your order details, the terms and conditions provided by Springer, and the payment terms and conditions.

All payments must be made in full to CCC. For payment instructions, please see information listed at the bottom of this form.

License Number	2658400521738
License date	Apr 29, 2011
Licensed content publisher	Springer
Licensed content publication	Journal of Atmospheric Chemistry
Licensed content title	Laboratory spectroscopic studies of atmospherically important radicals using fourier transform spectroscopy
Licensed content author	P. T. Wassell
Licensed content date	Jan 1, 1989
Volume number	8
Issue number	1
Type of Use	Thesis/Dissertation
Portion	Figures
Author of this Springer article	No
Order reference number	
Title of your thesis / dissertation	Development of a Knudsen Cell Reactor for Measuring the Uptake of Atmospheric Gases on Particulate Matter
Expected completion date	May 2011

Estimated size(pages)	95
Total	0.00

USD Terms and Conditions

References

(1) Finlayson-Pitts, B. J.; Pitts, J. N. *Chemistry of the Upper and Lower Atmosphere: Theory, Experiments, and Applications*; Academic Press: San Diego, 2000.
(2) Rudich, Y. *Chemical Reviews* **2003**, *103*, 5097.
(3) Seinfeld, J. H.; Pandis, S. N. *Atmospheric Chemistry and Physics: From Air Pollution to Climate Change*; 2nd ed.; John Wiley & Sons Inc.: Hoboken, NJ, 2006.
(4) Cwiertny, D. M.; Young, M. A.; Grassian, V. H. *Annual Review of Physical Chemistry* **2008**, *59*, 27.
(5) Carlos-Cuellar, S.; Li, P.; Christensen, A. P.; Krueger, B. J.; Burrichter, C.; Grassian, V. H. *Journal of Physical Chemistry A* **2003**, *107*, 4250.
(6) Goss, K. U.; Schwarzenbach, R. P. *Environmental Science & Technology* **1999**, *33*, 4073.
(7) Golden, D. M.; Spokes, G. N.; Benson, S. W. *Angewandte Chemie International* **1973**, *12*, 534.
(8) *Applications of Chemical Kinetics*; Golden, D. M.; Manion, J. A., Eds.; JAI Press Inc.: Greenwich, CT, 1992; Vol. 1.
(9) *Heterogeneous Chemsitry on Global Stratospheric Particulate: Reaction of $ClONO_2$ and N_2O_5 on Sulfuric Acid Surfaces*; Golden, D. M.; Manion, J. A.; Reihs, C. M.; Tolbert, M. A., Eds.; Blackwell Scientific Publications: Oxford, 1994.
(10) Hatch, C. D.; Grassian, V. H. *Journal of Environmental Monitoring* **2008**, *10*, 919.
(11) Gasso, S.; Grassian, V. H.; Miller, R. L. *Elements* **2010**, *6*, 247.
(12) Claquin, T.; Schulz, M.; Balkanski, Y. J. *Journal of Geophysical Research-Atmospheres* **1999**, *104*, 22243.
(13) Krueger, B. J.; Grassian, V. H.; Cowin, J. P.; Laskin, A. *Atmospheric Environment* **2004**, *38*, 6253.
(14) Ramanathan, V.; Crutzen, P. J.; Kiehl, J. T.; Rosenfeld, D. *Science* **2001**, *294*, 2119.
(15) Sokolik, I. N.; Toon, O. B. *Nature* **1996**, *381*, 681.
(16) Jacobson, M. Z. *Journal of Geophysical Research-Atmospheres* **2001**, *106*, 1551.
(17) Ellison, G. B.; Tuck, A. F.; Vaida, V. *Journal of Geophysical Research-Atmospheres* **1999**, *104*, 11633.
(18) Krivacsy, Z.; Gelencser, A.; Kiss, G.; Meszaros, E.; Molnar, A.; Hoffer, A.; Meszaros, T.; Sarvari, Z.; Temesi, D.; Varga, B.; Baltensperger, U.; Nyeki, S.; Weingartner, E. *Journal of Atmospheric Chemistry* **2001**, *39*, 235.
(19) Facchini, M. C.; Fuzzi, S.; Zappoli, S.; Andracchio, A.; Gelencser, A.; Kiss, G.; Krivacsy, Z.; Meszaros, E.; Hansson, H. C.; Alsberg, T.; Zebuhr, Y. In *Joint Symposium on Atmospheric Chemistry and Climate Change* Seattle, Washington, 1998; Vol. 104, p 26821.
(20) Law, N. L.; Diamond, M. L. *Chemosphere* **1998**, *36*, 2607.
(21) Seisel, S.; Lian, Y.; Keil, T.; Trukhin, M. E.; Zellner, R. *Physical Chemistry Chemical Physics* **2004**, *6*, 1926.
(22) Rognon, P.; CoudeGaussen, G.; Revel, M.; Grousset, F. E.; Pedemay, P. *Sedimentology* **1996**, *43*, 359.
(23) Perry, K. D.; Cliff, S. S.; Jimenez-Cruz, M. P. *Journal of Geophysical Research-Atmospheres* **2004**, *109*.
(24) Michel, A. E.; Usher, C. R.; Grassian, V. H. *Geophysical Research Letters* **2002**, *29*.
(25) Michel, A. E.; Usher, C. R.; Grassian, V. H. *Atmospheric Environment* **2003**, *37*, 3201.

(26) Usher, C. R.; Michel, A. E.; Stec, D.; Grassian, V. H. *Atmospheric Environment* **2003**, *37*, 5337.
(27) Moise, T.; Rudich, Y. *Journal of Geophysical Research-Atmospheres* **2000**, *105*, 14667.
(28) Underwood, G. M.; Li, P.; Al-Abadleh, H.; Grassian, V. H. *Journal of Physical Chemistry A* **2001**, *105*, 6609.
(29) Underwood, G. M.; Song, C. H.; Phadnis, M.; Carmichael, G. R.; Grassian, V. H. *Journal of Geophysical Research-Atmospheres* **2001**, *106*, 18055.
(30) Grassian, V. H. *Journal of Physical Chemistry A* **2002**, *106*, 860.
(31) Goodman, A. L.; Underwood, G. M.; Grassian, V. H. *Journal of Physical Chemistry A* **1999**, *103*, 7217.
(32) Goodman, A. L.; Bernard, E. T.; Grassian, V. H. *Journal of Physical Chemistry A* **2001**, *105*, 6443.
(33) Johnson, E. R.; Sciegienka, J.; Carlos-Cuellar, S.; Grassian, V. H. *Journal of Physical Chemistry A* **2005**, *109*, 6901.
(34) Dentener, F. J.; Carmichael, G. R.; Zhang, Y.; Lelieveld, J.; Crutzen, P. J. *Journal of Geophysical Research-Atmospheres* **1996**, *101*, 22869.
(35) Dentener, F. J.; Crutzen, P. J. *Journal of Geophysical Research-Atmospheres* **1993**, *98*, 7149.
(36) Underwood, G. M.; Miller, T. M.; Grassian, V. H. *Journal of Physical Chemistry A* **1999**, *103*, 6184.
(37) Usher, C. R.; Al-Hosney, H.; Carlos-Cuellar, S.; Grassian, V. H. *Journal of Geophysical Research-Atmospheres* **2002**, *107*.
(38) Davis, S. M.; Lunsford, J. H. *Journal of Environmental Science and Health Part a-Environmental Science and Engineering & Toxic and Hazardous Substance Control* **1976**, *11*, 735.
(39) Brasseur, G. P.; Orlando, J. J.; Tyndall, G. S. *Atmospheric Chemistry and Global Change*; Oxford University Press: New York, 1999.
(40) Al-Hosney, H. A.; Carlos-Cuellar, S.; Baltrusaitis, J.; Grassian, V. H. *Physical Chemistry Chemical Physics* **2005**, *7*, 3587.
(41) Chen, Z. M.; Jie, C. Y.; Li, S.; Wang, H. L.; Wang, C. X.; Xu, J. R.; Hua, W. *Journal of Geophysical Research-Atmospheres* **2008**, *113*.
(42) Goss, K. U. *Environmental Science & Technology* **1992**, *26*, 2287.
(43) Goss, K. U. *Environmental Science & Technology* **1993**, *27*, 2127.
(44) Goss, K. U.; Eisenreich, S. J. *Environmental Science & Technology* **1996**, *30*, 2135.
(45) Goss, K. U.; Schwarzenbach, R. P. *Journal of Colloid and Interface Science* **2002**, *252*, 31.
(46) Li, P.; Perreau, K. A.; Covington, E.; Song, C. H.; Carmichael, G. R.; Grassian, V. H. *Journal of Geophysical Research-Atmospheres* **2001**, *106*, 5517.
(47) Liu, Y.; Ma, J.; He, H. *Atmospheric Chemistry and Physics* **2010**, *10*, 10335.
(48) Navea, J. G.; Xu, S. H.; Stanier, C. O.; Young, M. A.; Grassian, V. H. *Atmospheric Environment* **2009**, *43*, 4060.
(49) Prince, A. P.; Kleiber, P. D.; Grassian, V. H.; Young, M. A. *Physical Chemistry Chemical Physics* **2008**, *10*, 142.
(50) Grassian, V. H. *International Reviews in Physical Chemistry* **2001**, *20*, 467.
(51) Keyser, L. F.; Leu, M. T.; Moore, S. B. *Journal of Physical Chemistry* **1993**, *97*, 2800.
(52) Keyser, L. F.; Moore, S. B.; Leu, M. T. *Journal of Physical Chemistry* **1991**, *95*, 5496.

(53) Caloz, F.; Fenter, F. F.; Tabor, K. D.; Rossi, M. J. *Review of Scientific Instruments* **1997**, *68*, 3172.
(54) Ward, J. W.; Mulford, R. N. R. *The Journal of Chemical Physics* **1967**, *47*, 1710
(55) Kennard, E. H. *Kinetic Theory of Gases*; McGraw-Hill Book Company: New York, 1938.
(56) O'Hanlon, J. F. *A User's Guide to Vacuum Technology*; 2nd ed.; John Wiley & Sons, Inc.: New York, 1989.
(57) Ideal Vacuum Products, LLC.
(58) Linstrom, P. J.; National Institute of Standards and Technology: 2008.
(59) Seisel, S.; Keil, T.; Lian, Y.; Zellner, R. *International Journal of Chemical Kinetics* **2006**, *38*, 242.
(60) Ullerstam, M.; Johnson, M. S.; Vogt, R.; Ljungstrom, E. *Atmospheric Chemistry and Physics* **2003**, *3*, 2043.
(61) Li, P.; Al-Abadleh, H. A.; Grassian, V. H. *Journal of Physical Chemistry A* **2002**, *106*, 1210.
(62) Natal-Santiago, M. A.; Dumesic, J. A. *Journal of Catalysis* **1998**, *175*, 252.
(63) Hautefeuille, P.; Chappuis, J. *Comptes Rendus Hebdomadaires des Seances de l'Academie des Sciences* **1881**, *92*, 80
(64) Wayne, R. P.; Barnes, I.; Biggs, P.; Burrows, J. P.; Canosamas, C. E.; Hjorth, J.; Lebras, G.; Moortgat, G. K.; Perner, D.; Poulet, G.; Restelli, G.; Sidebottom, H. *Atmospheric Environment Part a-General Topics* **1991**, *25*, 1.
(65) Graham, R. A.; Johnston, H. S. *Journal of Physical Chemistry* **1978**, *82*, 254.
(66) Noxon, J. F.; Norton, R. B.; Henderson, W. R. *Geophysical Research Letters* **1978**, *5*, 675.
(67) Noxon, J. F.; Norton, R. B.; Marovich, E. *Geophysical Research Letters* **1980**, *7*, 125.
(68) Platt, U.; Perner, D.; Winer, A. M.; Harris, G. W.; Pitts, J. N. *Geophysical Research Letters* **1980**, *7*, 89.
(69) Ishiwata, T.; Fujiwara, I.; Naruge, Y.; Obi, K.; Tanaka, I. *Journal of Physical Chemistry* **1983**, *87*, 1349.
(70) Pitts, J. N.; Biermann, H. W.; Atkinson, R.; Winer, A. M. *Geophysical Research Letters* **1984**, *11*, 557.
(71) Naudet, J. P.; Rigaud, P.; Pirre, M. *Journal of Geophysical Research-Atmospheres* **1989**, *94*, 6374.
(72) Neta, P.; Huie, R. E. *Journal of Physical Chemistry* **1986**, *90*, 4644.
(73) Imamura, T.; Rudich, Y.; Talukdar, R. K.; Fox, R. W.; Ravishankara, A. R. *Journal of Physical Chemistry A* **1997**, *101*, 2316.
(74) Rudich, Y.; Talukdar, R. K.; Imamura, T.; Fox, R. W.; Ravishankara, A. R. *Chemical Physics Letters* **1996**, *261*, 467
(75) Seisel, S.; Caloz, F.; Fenter, F. F.; vandenBergh, H.; Rossi, M. J. *Geophysical Research Letters* **1997**, *24*, 2757.
(76) Pitts, J. N.; Zielinska, B.; Sweetman, J. A.; Atkinson, R.; Winer, A. M. *Atmospheric Environment* **1985**, *19*, 911.
(77) Gross, S.; Bertram, A. K. *Journal of Physical Chemistry A* **2008**, *112*, 3104.
(78) Moise, T.; Talukdar, R. K.; Frost, G. J.; Fox, R. W.; Rudich, Y. *Journal of Geophysical Research-Atmospheres* **2002**, *107*.
(79) Gross, S.; Bertram, A. K. *Journal of Geophysical Research-Atmospheres* **2009**, *114*.
(80) Schott, G.; Davidson, N. *Journal of the American Chemical Society* **1958**, *80*, 1841

(81) Fenter, F. F.; Caloz, F.; Rossi, M. J. *Journal of Physical Chemistry* **1996**, *100*, 1008.
(82) Haynes, W. M.; Taylor and Francis Group, LLC: 2011.
(83) Rudich, Y.; Talukdar, R. K.; Ravishankara, A. R.; Fox, R. W. *Journal of Geophysical Research* **1996**, *101*, 21.023
(84) Talawar, M. B.; Sivabalan, R.; Polke, B. G.; Nair, U. R.; Gore, G. M.; Asthana, S. N. *Journal of Hazardous Materials* **2005**, *124*, 153.
(85) Wassell, P. T.; Wayne, R. P.; Ballard, J.; Johnston, W. B. *Journal of Atmospheric Chemistry* **1989**, *8*, 63.